Available online at www.sciencedirect.com

ScienceDirect

Journal of Magnesium and Alloys 12 (2024) 1774–1791

www.elsevier.com/locate/jma

Review

Towards designing high mechanical performance low-alloyed wrought magnesium alloys via grain boundary segregation strategy: A review

Zhi Zhang[a,b], Jinshu Xie[a,b], Jinghuai Zhang[a,*], Xu-Sheng Yang[b,c,**], Ruizhi Wu[a]

[a] *Key Laboratory of Superlight Material and Surface Technology, Ministry of Education, College of Materials Science and Chemical Engineering, Harbin Engineering University, Harbin 150001, China*

[b] *State Key Laboratory of Ultra-Precision Machining Technology, Department of Industrial and Systems Engineering, The Hong Kong Polytechnic University, Hung Hom, Kowloon, Hong Kong, China*

[c] *Hong Kong Polytechnic University Shenzhen Research Institute, Shenzhen 518060, China*

Received 27 November 2023; received in revised form 4 March 2024; accepted 27 March 2024
Available online 12 April 2024

Abstract

Low-alloyed magnesium (Mg) alloys have emerged as one of the most promising candidates for lightweight materials. However, their further application potential has been hampered by limitations such as low strength, poor plasticity at room temperature, and unsatisfactory formability. To address these challenges, grain refinement and grain structure control have been identified as crucial factors to achieving high performance in low-alloyed Mg alloys. An effective way for regulating grain structure is through grain boundary (GB) segregation. This review presents a comprehensive summary of the distribution criteria of segregated atoms and the effects of solute segregation on grain size and growth in Mg alloys. The analysis encompasses both single element segregation and multi-element co-segregation behavior, considering coherent interfaces and incoherent interfaces. Furthermore, we introduce the high mechanical performance low-alloyed wrought Mg alloys that utilize GB segregation and analyze the potential impact mechanisms through which GB segregation influences materials properties. Drawing upon these studies, we propose strategies for the design of high mechanical performance Mg alloys with desirable properties, including high strength, excellent ductility, and good formability, achieved through the implementation of GB segregation. The findings of this review contribute to advancing the understanding of grain boundary engineering in Mg alloys and provide valuable insights for future alloy design and optimization.

Keywords: Magnesium alloys; Grain boundary segregation; High strength; High plasticity; High formability.

1. Introduction

Low-alloyed magnesium (Mg) alloys have emerged as one of the most promising candidates for high-performance Mg alloys due to their lower density and cost as compared to other materials [1–4]. The addition of low-content alloying elements ($\leq$ 5 wt%) in these alloys can offer advantages such as avoidance of large eutectic phases and reduced thermal processing temperature, facilitating large-scale production and contributing to energy-saving and emission reduction [5–9]. However, the hexagonal close-packed structure of Mg alloys presents challenges such as low plasticity and poor formability at room temperature (RT) [10–12]. Moreover, low-alloyed Mg alloys face greater challenges in achieving high absolute strength and thermal stability compared with high-alloyed Mg alloys.

Extensive research efforts have been dedicated to developing high mechanical performance low-alloyed Mg alloys [5,13–16]. Certain common characteristics and rules can be

* Corresponding author.
** Corresponding author at: State Key Laboratory of Ultra-precision Machining Technology, Department of Industrial and Systems Engineering, The Hong Kong Polytechnic University, Hung Hom, Kowloon, Hong Kong, China.
E-mail addresses: zhangjinghuai@hrbeu.edu.cn (J. Zhang), xsyang@polyu.edu.hk (X.-S. Yang).

https://doi.org/10.1016/j.jma.2024.03.016

summarized through a review of the literature. Firstly, unlike common high-strength Mg-Gd/Y alloys via high alloying, achieving high strength in low-alloyed Mg alloys cannot rely solely on precipitation strengthening. The precipitation strengthening increment in Mg-Gd/Y alloys can reach as high as 143 MPa [17,18], while the strengthening effect resulting from precipitation is generally challenging to exceed 50 MPa in the Mg alloys with relatively low alloying content. For example, Bian et al. [19] improved the yield strength (YS) of Mg-1.3Al-0.8Zn-0.7Mn-0.5Ca (wt%) alloy from 177 MPa to 238 MPa by a 170 °C bake-hardening treatment, and the bake hardenability of this alloy is only about 40 MPa. However, there are some exceptions, such as Mn-containing Mg alloys that exhibit relatively high precipitation strengthening effects due to the dispersed distribution of refractory particles [5]. Nonetheless, this approach is limited by strict alloying requirements and harsh processing techniques.

Secondly, introducing fine-grained (about 5 μm and below) or heterogeneous-grained structure (such as bimodal structure and gradient structure) is one of the key factors in obtaining high mechanical performance low-alloyed Mg alloys [11,20–27]. Mg alloys exhibit more significant fine-grained strengthening effects as compared to Al alloys, mainly due to their higher k values (Hall-Petch slope) [28,29]. For instance, the k value of pure Mg (average grain size: ≥ 2 μm) is 280∼300 MPa $\mu m^{1/2}$ [30,31], while that of pure Al (average grain size: ≥ 1 μm) is 25∼70 MPa $\mu m^{1/2}$ [32]. This strong fine-grain strengthening effect provides the opportunities for the design of high-strength low-alloyed Mg alloys. Additionally, the introduction of some special-grained structure (such as bimodal grain structure) has shown potential for simultaneously improving the strength and ductility in Mg alloys [23,33]. For example, previous studies by Wang and colleagues have successfully implemented bimodal grain structure into several Mg alloys (such as AZ91 and Mg-8Al-2Sn-1Zn (wt%) alloys) by hard plate rolling, resulting in excellent strength-ductility combination [34–37].

Lastly, dislocations not only contribute to strengthening effect, but also play a role in plastic deformation of Mg alloys. The strengthening increment caused by dislocations (σ_d) would be proportional to the principal square root of the dislocation density (ρ) [38]:

$$\sigma_d = M\alpha Gb\sqrt{\rho} \quad (1)$$

where M is the Taylor factor, α is a constant (0.2), G is the shear modulus of Mg (about 16.8 GPa), and b is the Burgers vector of the gliding (about 0.32 nm). Dislocation strengthening is a crucial method for enhancing the strength of low-alloyed Mg alloys. Pan et al. [5] prepared a high-strength low-alloy Mg-1.0Ca-1.0Al-0.2Zn-0.1Mn (wt%) alloy through low-speed hot extrusion, where the strengthening increment caused by dislocations is about 115 MPa. However, an excessive dislocation density would lead to the dramatic reduction in plasticity at RT emphasizing the importance of appropriate dislocation configuration for the design of high mechanical performance Mg alloys suitable for engineering applications.

It is evident that if both dislocation configuration and grain structure can be controlled simultaneously, high mechanical performance Mg alloys have the opportunity to be designed. Grain boundary (GB) segregation has garnered significant attention in recent years as an effective strategy for regulating microstructures of low-alloyed Mg alloys [39]. However, studies on solute segregation have primarily focused on nano-scale structural characterization (such as distribution of segregated atoms) [40,41], with limited connection to microstructures and macroscopic mechanical properties. In this work, we not only summarize the distribution criteria of segregated atoms but also examine the effects of solute segregation on the grain size and growth of Mg alloys. The analysis encompasses both single element segregation and multi-element co-segregation behavior, considering at coherent interfaces and incoherent interfaces. Moreover, we propose strategies for designing high mechanical performance Mg alloys with superior properties, including high strength, excellent ductility, and good formability, through GB segregation. The review aims to provide valuable guidance for the design of high mechanical performance low-alloyed Mg alloys.

2. Interface segregation behavior of Mg alloys

2.1. Segregation sites and segregation level

Solute segregation mainly occurs in GBs and fully coherent twin boundaries (TBs) [40–43]. At present, many elements (such as Ag, Al, Bi, Ca, Mn, Zn) have been proven to exhibit certain segregation effects in Mg alloys under specific condition. The segregation sites of solute element is closely related to the radius of the atoms [44,45]. The atomic radius of Mg is about 1.6 Å. Fig. 1 shows the atomic radius mismatch values between common alloying atoms and Mg atom [2]. The Ag, Al, Be, Cd, Ga, Ge, Li, Mn, Sb, Si, Sn, Ti, and Zn atoms show smaller atomic radius than Mg atom radius, while the Ca, Pb, In, Tl, and rare earth (RE, such as Ce, Dy, Er, Gd, Ho, Lu, Nd, Sc, Sm, Y, Yb) atoms have larger atomic radius than Mg atom radius. If the radius of the segregated atom is greater/less than that of Mg, it is called a "large''/"small'' atom. The "large'' atoms tend to occupy the "extension position'', while the "small'' atoms tend to occupy the "contraction position''. For example, Xiao et al. [46–48] have reported the interface segregation behavior of Mg-Ag alloy. As a conventional rule, Ag, as a "small'' atom, is more likely to occupy the contraction position of the local strain field. Wang et al. [49] found that Y atoms ("large'' atom) segregate to the extension sites at {10–12} coherent twinning boundary (TB) segment.

Of course, there are also unusual phenomena in some Mg alloys. For example, He et al. [40] reported an unusual solute segregation phenomenon in the Mg-0.4Bi (at%) alloy (Fig. 2). The Bi atoms with a larger radius (1.7 Å) unexpectedly segregate to compression sites of {10–11} fully coherent TBs instead of the extension or compression sites of {10–12} fully coherent TBs. This segregation is not dominated by traditional elastic strain minimization but by chemical bonding (in-

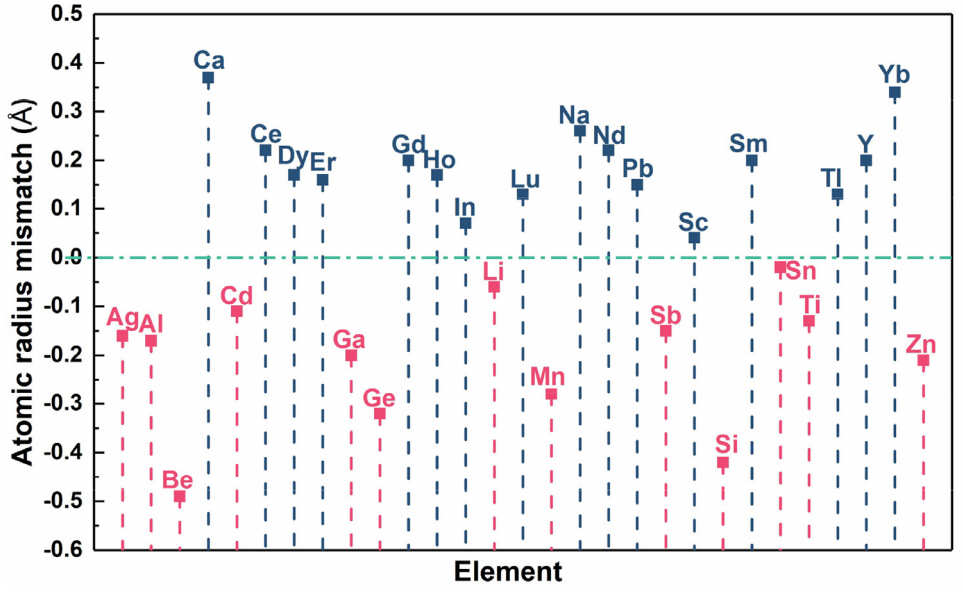

Fig. 1. The atomic radius mismatch values between alloying atoms and Mg atom [2].

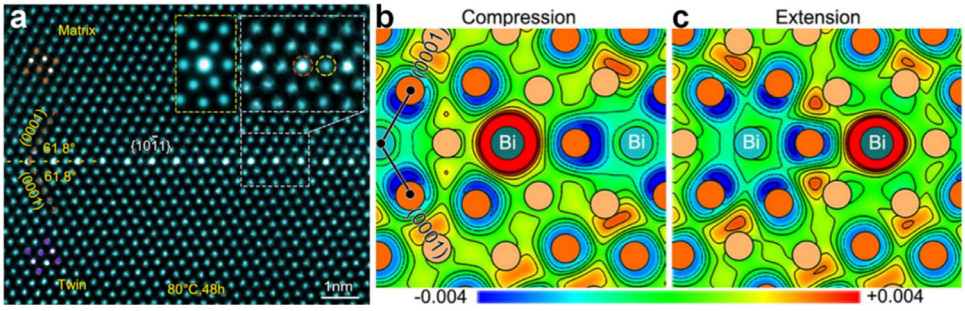

Fig. 2. (a) Periodic segregation of Bi atoms in{10–11} coherent TB. (b,c) (11–20) plane contour maps of DECD of Bi atoms segregated in {10–11} CTB [40]. (Reprinted from Nat. Commun. 12, Unusual solute segregation phenomenon in coherent twin boundaries, 722, Copyright 2022, open access.)

cluding coordination and solute electronic configuration). As shown in Fig. 2(b,c), the contour maps of differential electron charge density (DECD) indicate that more valence electrons would be trapped when Bi segregate to the compression site.

Calculating the cohesive energy (E_{coh}) and segregation energy (E_{seg}) of the interface is a more direct means to evaluate the segregation tendency. In terms of twinning, E_{coh}, which is used to evaluate the stability of TBs, can be calculated as [44,49,50]:

$$E_{coh} = \left[E_{TB}(Mg_{n-m}X_m) - (n-m)E^{Mg}_{atom} - mE^{X}_{atom}\right] \quad (2)$$

where $E_{TB}(Mg_{n-m}X_m)$ is the total energy of a cell with the faceted TB and m segregated X atoms, $E_{atom}{}^{Mg}$ and $E_{atom}{}^{X}$ are the energies of isolated Mg and solute atom X. A negative value of E_{coh} is more conducive to the stability of TB segregation. E_{seg}, which is defined as the reduction in total system energy when solute atoms segregate to TB, can be calculated as [44,50–52]:

$$E_{seg} = \left\{[E_{TB}(Mg_{N-m}X_m) - E_{TB}(Mg_N)] - m[E_{matrix}(Mg_{M-1}X) - E_{matrix}(Mg_M)]\right\}/m \quad (3)$$

where $E_{TB}(Mg_N)$ is the total energy of a pure Mg super-cell containing TB, $E_{matrix}(Mg_{M-1}X)$ is the total energy of a TB-free cell with (M-1) Mg atoms and 1 segregated atom, and $E_{matrix}(Mg_M)$ is the energy of a pure Mg super-cell with M Mg atoms. Ju et al. [53] analyzed the E_{coh} and TB E_{seg} for various alloying elements in Mg, and found that E_{seg} decreases approximately linearly as the atomic size difference between Mg atom and solute atoms increases (Fig. 3a,b), while solute atoms with higher electronegativity than Mg tend to occupy compression positions (Fig. 3c). Taking all factors into consideration, the segregated atoms with smaller atomic radius than Pb (1.75 Å) tend to occupy the compression sites, while solute atoms with larger atomic radius than Pb tend to segregate at the extension sites.

Compared with single element segregation, multi-component segregation system is a more extensive and common system. Mg-Ca-Zn alloys [54,55], Mg-Mn-Nd alloys [41,56], Mg-RE-Zn alloys [57,58] and Mg-RE-Ag alloys [59–61] are the common ternary alloy systems with higher segregation level. These segregation systems are all systems in which "large'' atoms and "small'' atoms exist at the same time, and the atomic arrangement is often more complex. Still

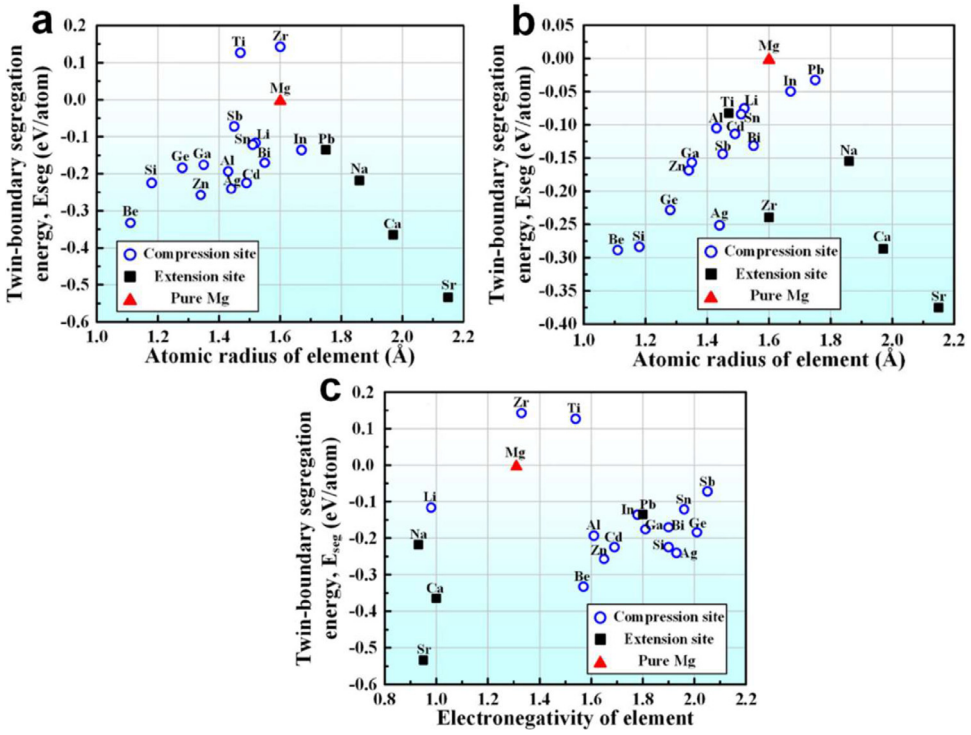

Fig. 3. Relationships between the atomic radius and (a) E_{seg} of {10–12} TB or (b) E_{seg} of {10–11} TB. (c) Relationship between the electronegativity of alloying elements and E_{seg} of {10–12} TB [53]. (Reprinted from J. Mater. Res. Technol. 24, First-principles study on the segregation behavior of solute atoms at {10–12} and {10–11} twin boundaries of Mg, 8563, Copyright 2023, open access.)

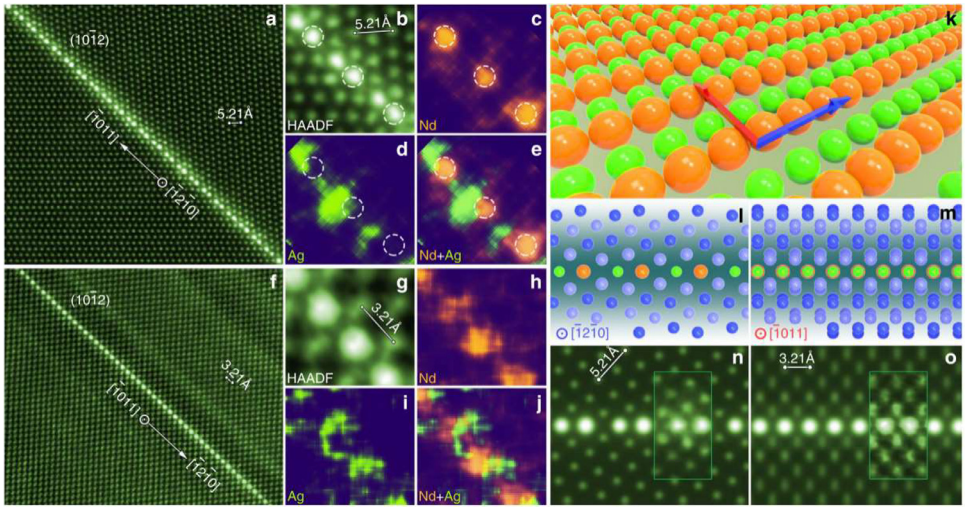

Fig. 4. Alternating distribution of Nd and Ag columns in a (10–12) TB [59]. Atomic-resolution (a-e) [−12–10] and (f-j) [−1011] HAADF-STEM image and corresponding atomic-resolution EDS maps. Dashed circles in (b-e) indicate extension sites. (k) Schematic diagram showing arrangement of Nd and Ag atoms within a (10–12) TB. Blue and red arrows indicate [−12–10] and [−1011] directions, respectively. Segregation layer viewed along (l) [−12–10] and (m) [−1011]. Simulated (n) [−12–10] and (o) [−1011] HAADF-STEM images, respectively. (Reprinted from Nat. Commun. 10, Direct observation and impact of co-segregated atoms in magnesium having multiple alloying elements, 3243, Copyright 2019, open access.)

taking coherent TBs as an example, Zhao et al. [59] directly observed the alternating distribution of Nd and Ag atoms in the TBs of the Mg-2.10Nd-3.01Ag-0.34Zr (wt%) alloys (Fig. 4). Nd atoms, as the "large'' atom, occupy the extension sites, while Ag atoms segregate to extension sites as the the "small'' atom. Nie et al. [44] also reported an unusual segregation mode in {10–12} TB of Mg-Gd-Zn alloy, and found that Zn atoms would occupy the compressed sites at the {10–12} TB in the Mg-Zn binary alloy, while both Zn and Gd atoms would segregate to the extension sites of the {10–12} TB in the Mg-Gd-Zn alloy (Fig. 5). In addition, the calculation method for the segregation energy of TB co-segregation of multiple elements was proposed to more accurate assessment of segregation locations [44], and the re-

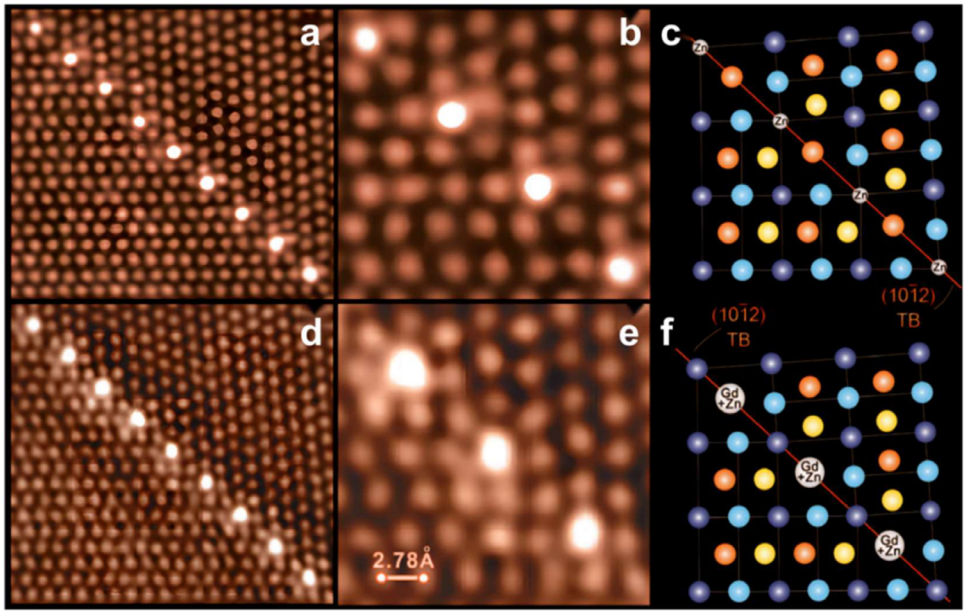

Fig. 5. HAADF-STEM images and schematic illustrations showing {10–12} TBs in the (a–c) Mg-1.9Zn (at%) alloy and (d–f) Mg-1.0Gd-0.4Zn-0.2Zr (at%) alloy [44]. (Reprinted from Science 340, Periodic segregation of solute atoms in fully coherent twin boundaries, 958, Copyright 2013, open access).

duction in the total energy per unit TB area (E_A) and per unit volume of the super-cell (E_V) can be calculated as:

$$E_A = \frac{C_{sol}^{TB} \times n \times E_{seg}}{a \times b} \tag{4}$$

$$E_V = \frac{C_{sol}^{TB} \times n \times E_{seg}}{a \times b \times c} = \frac{E_A}{c} \tag{5}$$

where *a, b, c* are the dimensions of super-cell, and *n* is the number of atoms in specific column.

The TBs belong to coherent interfaces, the segregation sites of solute atoms are generally relatively simple, while the segregation behavior of atoms at the GBs is often more complex and unpredictable. Xie et al. [62] reported the non-symmetrical segregation of solutes in periodic misfit dislocations separated tilt GBs in the Mg-2Nd-1Mn (wt%) alloy, and confirmed that elastic strain minimization promotes non-symmetrical segregation of solutes in four types of linear tilt GBs to generate ordered interfacial superstructures (Fig. 6). This also indicates that the periodic distribution of interface segregation is not limited to highly symmetrical coherent interfaces (such as TBs), but widely exists in various types of GBs. It is worth noting that the complex GBs structure corresponds to a variety of segregation types, which also suggests the more possibility of increasing the level of GB segregation compared to TB segregation. In addition, the segregation levels of high-angle GBs are often different [63,64]. Zhao et al. [64] observed the different high-angle GBs have different GB segregation levels. Therefore, the determination of GB segregation level requires counting multiple GBs to give statistical results [65,66].

Currently, studies have confirmed that multiple co-segregation on GBs can effectively improve the segregation level. Zeng et al. [54] compared the GB segregation behavior of cold-rolled Mg-0.3Zn-0.1Ca, Mg-0.4Zn and Mg-0.1Ca (at%) alloys, and found that the co-segregation effect of Zn and Ca is significantly better than that of single element segre-

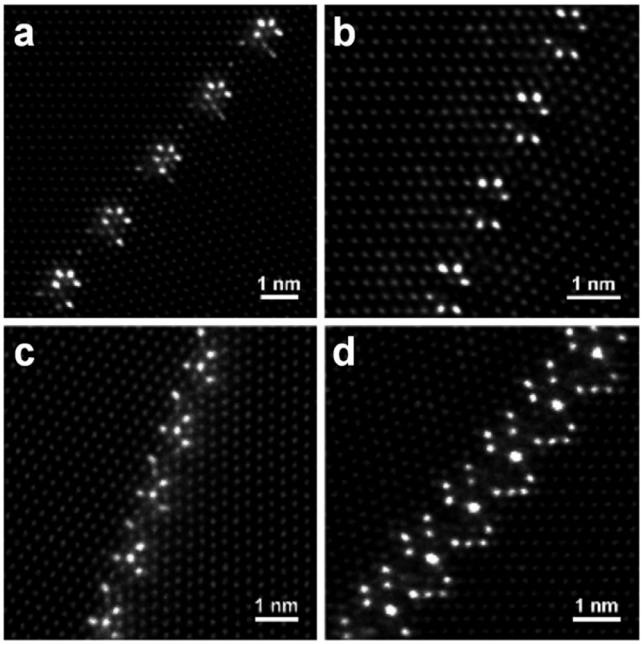

Fig. 6. Atomic-scale HAADF-STEM images showing segregation of solutes in four types of linear tilt GBs viewed along the <11–20> tilt axis [62]. (a) Asymmetric tilt GBs-type 1 (tilt angles $\theta1 = 51$ ° and $\theta2 = 79$ °); (b) asymmetric tilt GBs-type 2 (tilt angles $\theta1 = 116$ ° and $\theta2 = 17$ °); (c) symmetric tilt GBs-type 3 (tilt angles $\theta1 = 20.5$ ° and $\theta2 = 20$ °); (d) symmetric tilt GBs-type 4 (tilt angles $\theta1 = 51$ ° and $\theta2 = 49$ °). (Reprinted from Nano Lett. 21, Nonsymmetrical segregation of solutes in periodic misfit dislocations separated tilt grain boundaries, 2870, Copyright 2021 form American Chemical Society).

gation. In addition, the ternary co-segregation phenomenon in Mg alloys has also been reported from time to time. Pei et al. [67] analyzed the co-segregation phenomenon of Mg-3Al-1Zn-0.4Mn-0.3Ca (wt%, AZMX3100) alloys with or without solution treatment before rolling. The AZMX3100 alloy without solution treatment exhibits stronger Al, Ca, and Zn GB co-segregation. From an energy perspective, the co-segregation of the "small'' atoms of Al and Zn and the "large'' atoms of Ca (the large and small atoms are relative to the Mg atom) would be more effective in limiting grain growth than the segregation of the atoms alone, because it helps to greatly reduce GB energy and reduce the fluidity of GBs. Our study also found a co-segregation of Zn, Ca and Sm, and the segregation effect is significantly stronger than the co-segregation of Zn and Ca [68]. This is related to the elastic strain minimization caused by size mismatch between solute atoms and Mg atoms. On the one hand, due to the complexity of elemental components and GB structures, it is very difficult to directly observe the segregation behavior/sites of GBs. The comparison of these GB segregation levels generally relies on the 3D-APT and TEM-EDS results [69–71,56,72]. On the other hand, it is precisely the complex structure of GBs that provides more possibilities for increasing the level of GB segregation.

Based on GB equilibrium model, several researchers have devoted great efforts to evaluate GB segregation behavior via using molecular dynamics (MD) simulations or density functional theory (DFT) [73–76,39,77]. Langmuir-McLean segregation isotherm is a common model for studying single element segregation, and the relevant equation is as follows [78–82]:

$$c^i_{GB} = \frac{c^i_0 exp\left(\frac{E_{seg}}{k_B T}\right)}{1 - c^i_0 + c^i_0 exp\left(\frac{E_{seg}}{k_B T}\right)} \tag{6}$$

where c^{i}_{GB} is the GB-riched equilibrium concentration, k_B is the Boltzmann constant, and c^{i}_{0} is the initial concentration of segregated element in the bulk matrix. Based on the model, Koju et al. [78] revealed the segregation level and free energy of Mg GB segregation in Al-Mg alloys by MD, and also observed a tendency for forming clusters in high-angle GBs, indicating a more complex and peculiar segregation feature of GBs. Guttmann and McLean proposed [83–85] the Guttmann model of GB segregation for multi-component systems, and derived the following segregation equation:

$$\frac{c^i_{GB}}{c^1_{GB}} = \frac{c^i_0}{c^1_0} exp\left(-\frac{E_{seg(i\to 1),0} - 2\alpha^1_{ii} c^i_{GB} + \sum_{j=2\ldots N;\, j\neq 1} \alpha^2_{ij} c^j_{GB}}{RT}\right) \tag{7}$$

where $\alpha_{ii}{}^{1}$ is the interaction between the 1-st and i th elements, and $\alpha_{ij}{}^{2}$ denotes the relative interaction between i th and j-th elements. If these two interaction constant is 0, the Eq. (7) could be transformed into Eq. (6).

A classic example where GB segregation of two solutes can enhance each other is the segregation behavior of Ni and Sb in Fe (*bcc*). Gutmann et al. [86–88] quantitatively explained that this segregation behavior is the result of attractive interactions between Ni and Sb atoms. However, the conclusion is challenged by an experimental phenomenon, i.e., the varieties of Sb concentration cannot affect Ni segregation [89–92]. Relevant research ultimately proved that this is mainly due to the site competition between the trace impurities C and Ni in the material. This also once again verified the Gutmann model. These studies provide a reference for understanding the segregation behavior of multi-component alloys in Mg alloys, indicating that GB segregation of multi-component Mg alloys needs to consider a variety of factors, including but not limited to the following points. (a) Segregation tendency of solute atoms. As mentioned before, size effect and electronegativity are one of the bases for interpretation of segregation tendency. In addition, the enthalpy of mixing (ΔH_{mix}) calculated by Miedema's model between Mg atom and segregated atom could also evaluate the segregation tendency, and the negative values can be considered to have segregation tendency. For example, we previously reported a Er segregation in Mg alloys, and the ΔH_{mix} between Mg and Er atoms is −5 kJ mol^{-1} [12]. (b) The varieties of matrix composition caused by chemical reactions (such as forming intermetallics during casting, solid solution, and aging precipitation). When evaluating GB segregation behavior, one should focus on the content of segregable solute atoms in the matrix rather than the nominal composition. (c) Site competition of different segregated elements. There is site competition among solute atoms with the similar nature during the segregation process. In addition to the site competition between C and Sb mentioned above [88,89], similar site competition phenomena also exist in Mg alloys. The APT results of Pei et al. [67] show the "small" atoms (Al and Zn atoms) have peak values at the same position, indicating a site composition between Al and Zn atoms. (d) Interaction of different elements. The ΔH_{mix} values between different atoms can also be used to reveal co-segregation effect. The ΔH_{mix} of Zn and Gd atoms is −31 kJ mol^{-1}, which is larger than those of other combinations (Mg-Zn: −4 kJ mol^{-1} and Mg-Gd: −6 kJ mol^{-1}). Therefore, these is a strong attraction between Zn and Gd atoms, which tends to cause Zn and Gd co-segregation preferentially in Mg-Gd-Zn alloys [93–96].

2.2. Effects of GB segregation on static recrystallization and grain growth

In terms of Mg alloys, the role of the GB segregation is mainly reflected in regulating the static recrystallization process, grain growth and texture evolution during the annealing process. GB segregation can effectively affect recrystallization behavior and control grain growth [97]. On the one hand, GB segregation can inhibit the preferential growth of grains and weaken the texture. The solute drag pressure (P_{d}) can be evaluated through the Cahne-Lückee-Stuwe (CLS) model [98–103]:

$$P_d = \frac{\alpha \upsilon X_m}{1 + \beta^2 \upsilon^2} \tag{8}$$

$$\alpha = \frac{4(RT)^2\delta}{V_m G_{seg} D_1}\left(\frac{1}{a^3 - a}\right) \tag{9}$$

$$a = -\frac{RT}{G}\ln\left(\frac{D_1}{D_{gb}}\right) \tag{10}$$

$$\frac{\alpha}{\beta^2} = \frac{2G_{seg}D_{gb}}{V_m \delta a}\left(1 - \frac{D_1}{D_{gb}}\right) \tag{11}$$

where v is the boundary velocity, X_m is the matrix concentration, V_m is the molar volume, G_{seg} is the segregation free energy, D_l is the lattice diffusion coefficient, D_{gb} is the GB diffusion coefficient [103–105], δ is the width of the GB, R is the universal gas constant and T is the absolute temperature. In addition, experimental evidence can also confirm the positive correlation between segregation content and drag force. For example, Zeng et al. [54] studied the static recrystallization behavior and texture evolution of cold-rolled Mg-0.3Zn-0.1Ca, Mg-0.4Zn, and Mg-0.1Ca (at%) alloys during annealing. Quasi-*in-situ* EBSD analysis of annealed samples found that in the early stage of the recrystallization process, the initial grains of these three alloys show a relatively random orientation; however, as the recrystallized grains form and grow, the grains of all orientations in the ternary alloy grow uniformly and form a weaker texture, while preferential growth of recrystallized grains with specific orientations occurs in these two binary alloys. At the same time, the average grain size of the ternary alloy at each recrystallization stage is smaller than those of the binary alloys, and the grain size distribution is more concentrated. GB segregation are observed in all three alloys, and Zn and Ca atoms in the Mg-Zn-Ca alloy have a stronger segregation effect than Zn or Ca atoms alone in the Mg-Zn/Ca alloys. This strong co-segregation significantly reduces GB mobility during recrystallization and growth process by decreasing GB energy and enhancing solute drag effects, inhibiting grain growth into preferable orientation (i.e., basal texture orientation) [106,107]. The well-known parabolic kinetic model is often used to evaluate the grain growth kinetics [108–113]:

$$\ln(k) = \ln k_0 - \frac{Q}{RT} \tag{12}$$

where k is the kinetic parameter related to GB mobility, k_0 is the pre-exponential constant, and Q is the grain growth activation energy. Hoseini-Athar et al. [114,115] compared the activation energies of four Mg-Gd-Zn alloys, and found that the Mg-2Gd-1Zn (wt%) alloy containing higher segregation shows the highest Q (109 kJ/mol), indicating a lower mobility of the GBs.

On the other hand, higher GB segregation levels cloud still limit the growth of some grains at higher annealing/thermal processing temperatures (usually greater than 400 °C), forming a grain structure with a mixture of abnormally large grains and fine grains instead of all coarse grains. Basu et al. [116] compared the GB segregation levels of Mg-1Gd and Mg-1Dy (wt%) alloys and found that Gd has a stronger GB segregation tendency. The basal texture intensity of the Mg-1Gd alloy annealed at 623 K is 2.7 times that of random distribution and its basal texture intensity is 4.3 times that of random distribution when annealed at 723 K, while the Mg-1Dy alloy with weaker segregation level does not show such obvious texture difference. This phenomenon is caused by the abnormal grain growth of strongly segregated Mg-1Gd alloy during high-temperature annealing. For the Mg-1Gd alloy, annealing at higher temperature is easy to overcome the hindrance of GB segregation, allowing certain grains with higher GB migration to grow preferentially. The preferential growth of grains engulfs the surrounding small grains, which is a spontaneous process of reduced free energy, and escapes the control of GB segregation, while the remaining small grains are still controlled by segregation and grow slowly, consequently resulting in the abnormal grain growth behavior and the formation of non-uniform/heterogeneousgrained structure [117–124].

These two aspects seem to be contradictory, but in fact, the effect of solute segregation on grain growth is determined by the level of GB segregation and annealing temperature. In response to this problem, Lücke and Stüwe [99] proposed the theory of impurity controlled GB motion in the 1970s. Pei et al. [67,125–128] used it to explain the phenomenon of grain growth under segregation (Fig. 7). They prepared an AZMX3100 alloy with a high level of Al/Zn/Ca co-segregation, and annealed it at 350 °C and 450 °C for 4 h to compare the grain growth under the two annealing modes. At the lower annealing temperature of 350 °C, migration kinetics are thought to be controlled by solute diffusivity at GBs, resulting in a low-rate drag migration. In contrast, the sample annealed at 450 °C exhibits a modified growth mode characterized by a transition from a low rate of drag migration to a free migration mode with a higher growth rate. This transition, associated with a jump in migration velocity, only applies to unusually large grains surrounded by much smaller grains, where the acting driving force at the boundary exceeds a certain threshold enough to overcome solute resistance, so that the boundary can detach itself from solute pinning and migrate rapidly. Further growth of these grains is always determined by the actual acting driving force, caused by local grain size advantages. It is worth noting that although the driving force for large grain migration increases at 450 °C, the small grains are still pinned by the GB segregation atmosphere to limit their growth. Some researchers have also revealed this phenomenon from other perspectives. Kim et al. [129–132] found that the phase-field model can be used to accurately and quantitatively describe GB motion under GB segregation conditions, and simulated the relationship between grain growth and GB segregation in a two-dimensional polycrystalline system, thereby confirming that the solute resistance effect can cause abnormal growth of grains. The initial average grain size also has a profound effect on the grain growth pattern. The smaller the average grain size, the higher the density of abnormally grown grains. When the initial grain size exceeds the critical grain size, abnormal grain growth would not occur.

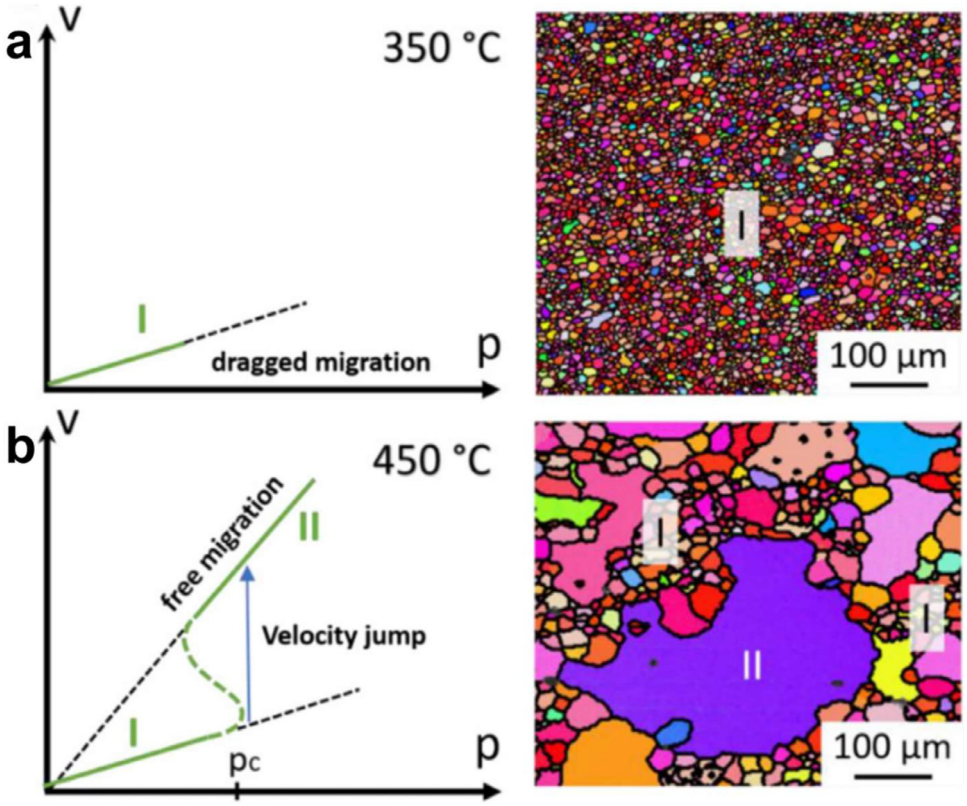

Fig. 7. Schematic drawing of the GB migration rate (v) vs. the driving force (p) illustrating two types of grain growth observed in Ref. [67]. (a) Solute drag-controlled migration during annealing at 350 °C giving rise to uniform grain growth at a low velocity. (b) Transition to rapid (free) migration exhibited by very large grains (region II), induced by raising the annealing temperature to 450 °C. (Reprinted from Acta Mater., 208, Grain boundary co-segregation in magnesium alloys with multiple substitutional elements, 116,749, Copyright 2021, with permission from Elsevier.)

3. GB segregation strategy for designing low-alloyed Mg alloys with high plasticity

Although the effect of GB segregation on plasticity in Mg alloys is not fully understood, it is generally considered to be positively correlated. The beneficial effects of GB segregation are mainly reflected in the following two aspects. Firstly, solute segregation can facilitate the nucleation of non-basal dislocations at GBs. Somekawa et al. [133–135] found that GBs with Y segregation have several prismatic $<a>$ dislocations, indicating that such GBs composed of atomically ordered steps become nucleation sites for non-basal dislocations. Our group [136,137] and Zhu et al. [138] also observed non-basal dislocations nucleating from GBs, and suggested that these dislocations are activated by GB segregation and local stress fields. The specific activation mechanisms are complex and variable, which is related to GB characteristics, segregation behavior, etc. An activation model of $<c+a>$ dislocations in the tensile twinning boundaries containing Zn/Ca segregation proposed by Basu et al. [139,140] could be used to briefly explain the behavior (Fig. 8). The Zn and Ca segregation would effectively lower the overall stacking-fault energies in Mg [141], which is beneficial to the formation of I_1 stacking fault ($\frac{1}{6}[20\bar{2}3]$). The I_1 stacking fault can potentially act as a stable $<c+a>$ dislocation-emission source, and the following dislocation reaction occurs [142,143]:

$$\frac{1}{6}[20\bar{2}3] \rightarrow \frac{1}{6}[2\bar{2}0\bar{3}] + \frac{1}{3}[\bar{2}113] \tag{13}$$

The Burgers vector of sessile stair-rod dislocation ($\frac{1}{6}[2\bar{2}0\bar{3}]$) is of the same nature as the bounding I_1 partial but with an opposite sign. If the applied stress is sufficient, a $<c+a>$ dislocation loop moving in the pyramidal plane would be eventually generated (Fig. 8c). However, there is currently no more intuitive atomic-scale evidence confirming the inevitable relationship between segregated atoms and dislocation nucleation. *In-situ* HR-TEM observation at grain boundaries is expected to be an effective way to track the formation of non-basal dislocation, and similar methods were used in the Refs. [144–146]. In addition, the geometric phase analysis (GPA) method could also be used to evaluate the local microscopic strain to assist the *in-situ* observation [147].

Secondly, segregation would effectively improve the cohesion of GBs, thereby delaying fracture and improving plasticity. Nandy et al. [148] found that GB co-segregation of Al/Zn/Ca elements has obviously higher segregation level than Ca single segregation, resulting in a decrease in the fraction of GB de-cohesion from 27% to 6% under 5% strain. Kula et al. [149–151] introduced the segregation of Y/Gd atoms to the GBs, suppressing intergranular failure of Mg-Y/Gd alloys. In the previous study, we compared Mg-Er

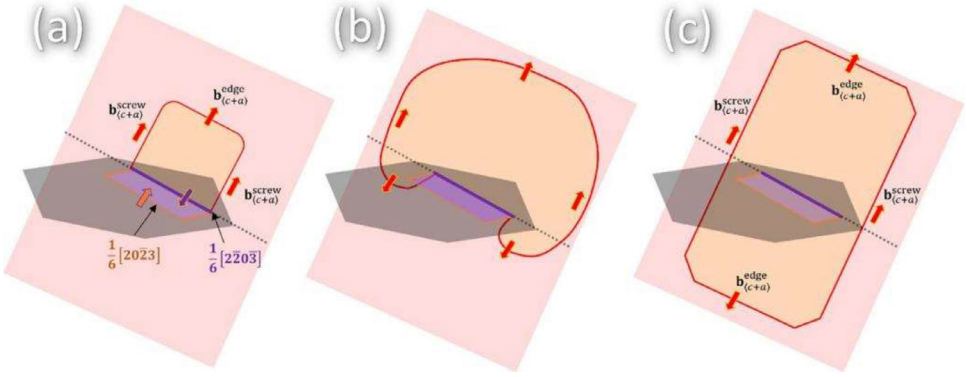

Fig. 8. Detailed schematic of $<c + a>$ slip generation from I_1 stacking faults [139]. (Reprinted from Acta Mater., 229, Segregation-driven exceptional twin-boundary strengthening in lean Mg-Zn-Ca alloys, 117,746, Copyright 2022, with permission from Elsevier.)

Table 1
GB segregation content and elongation of several Mg alloys.

Alloy composition (wt%)	States	GB segregation content (at%)	Elongation (%)	Refs.
Mg-2Er (HT300)	Extrusion+annealing (300 °C, 1 h)	2.2Er	47	[12]
Mg-2Er (HT360)	Extrusion+annealing (360 °C, 0.5 h)	0.5Er	36	
Mg-3Al-1Zn-1Mn-0.5Ca (AZMX3110)	Twin-roll casting (TRC) process	0.4Zn + 0.3Ca + 0.15Al	17	[65]
Mg-1Zn-0.3Ca	Extrusion Pillars (diameter of 2 μm)	1.45Zn + 0.95Ca	22	[139]
Pure Mg	Extrusion Pillars (diameter of 2 μm)	-	18	
Mg-0.1Ca	Rolling (450 °C, reduction: 90%)	0.62Ca	25	[148]
Mg-2Al-1Zn-0.1Ca		3.2Al+1.8Zn+0.4Ca	34	
Mg-1Zn (Z1)	As-extrusion (400 °C, speed: 1 mm/s)	low	18	[157]
Mg-1Zn-0.3Ca		1.3Zn + 0.3Ca	22	
Mg-1Zn-0.3Nd		1.6Zn + 1.2Ce	22	
Mg-1Zn-0.3Ce (ZCe10)		4.0Zn + 1.0Ca	31	
Mg-1Zn-0.2Ce	As-extrusion (450 °C, speed: 1 mm/s, ratio: 30)	1.5Zn + 0.5Ce	48	[158]
Mg-1Zn-0.2Ce-0.4Ca		3.3Zn + 2Ca+ 0.5Ce	56	

alloys with different GB segregation levels and found that higher GB segregation levels often correspond to lower fraction of GB cracking under similar grain characteristics [12].

In fact, not all GB segregation is beneficial to plasticity. GB embrittlement is an adverse effect of GB segregation, which is seldom mentioned in Mg alloys but has been reported in other structural metals [152]. In general, if the boundary cleavage becomes energetically conducive to dislocation emission (or blunting mechanisms), these GBs show embrittlement [153]. The energetic barrier for cleavage is the GB cohesion energy (E_{GBC}) mentioned above, which can be expressed as [154,155]:

$$E_{GBC} = 2\gamma_S - \gamma_{GB} \tag{14}$$

where γ_S is the surface energy, and γ_{GB} is the GB energy. Based on the Eq. (14), Gibson et al. [156] developed a model for evaluating the effect of solute segregation on E_{GBC} in the binary alloys, and found that GB embrittlement would be easily suppressed in the alloys with high E_{GBC} (Fig. 9). GB embrittlement induced by segregation may also exist in Mg alloys and needs further study.

At present, several high-plasticity Mg alloys based on GB segregation design have been reported, as listed in Table 1. It is obvious that in Mg alloys of similar state, the elonga-

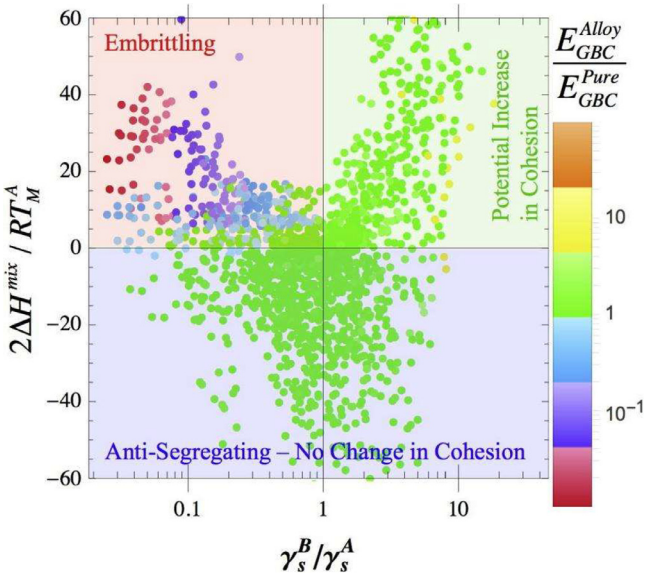

Fig. 9. A GB cohesion map of different segregation pairs [156]. Alloy pairs are placed upon the map according to the heat of mixing normalized by the melting temperature of the solvent and the ratio of the surface energy of the solute to the solvent. (Reprinted from Acta Mater. 95, Segregation-induced changes in grain boundary cohesion and embrittlement in binary alloys, 152, Copyright 2021, with permission from Elsevier.)

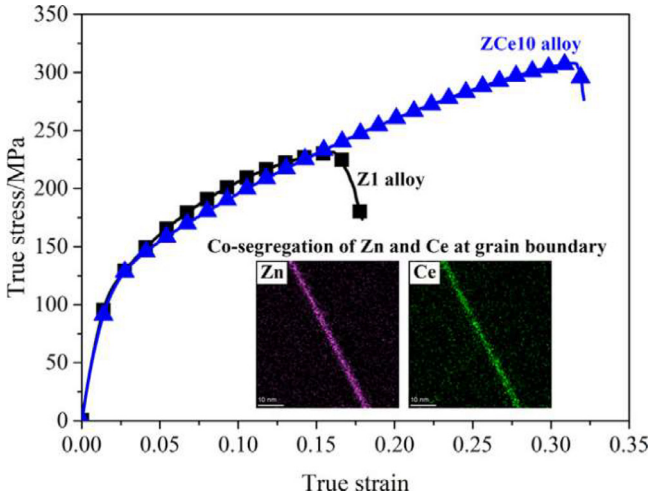

Fig. 10. True stress-strain curves of Mg-1Zn (Z1) and Mg-1Zn-0.3Ce (ZCe10) alloys, and GB segregation EDS maps of the ZCe10 alloy [157]. (Reprinted from Mater. Design 224, Influence of alloying element segregation at grain boundary on the microstructure and mechanical properties of Mg-Zn alloy, 152, Copyright 2022, open access.)

tion of the alloy is approximately positively correlated with the level of GB segregation. Qian et al. [157,158] developed several Mg-Zn alloys with different GB segregation levels, including Mg-1Zn (Z1), Mg-1Zn-0.3Ca, Mg-1Zn-0.3Ce (ZCe10), and Mg-1Zn-0.3Nd alloys (Table 1 and Fig. 10). Fig. 10 shows that the ZCe10 alloy with strong Zn and Ce GB co-segregation has a higher elongation than the Z1 alloy. In the previous work [12], we compared the high-plasticity Mg-2Er (wt%) alloys with similar grain sizes and different GB segregation, and confirmed that the GB segregation is beneficial to the improvement of plasticity at RT (Fig. 11). *In-situ* SEM results show the HT360 alloy with lower GB segregation has obvious GB cracks, and the cracked GBs fraction of HT360 alloy at different strain stages is significantly higher than that of HT300 alloy. These studies all reflect the beneficial effect of GB segregation on plasticity, and some other Mg alloys also have similar effects [159–161], indicating an effective strategy to improve plasticity via GB segregation. However, it must also be admitted that there is currently no clear intuitive evidence such as atomic scale observation for this strategy, which is related to the complexity of the GB structure and the instability and inhomogeneity of GB segregation.

4. GB segregation strategy for designing low-alloyed Mg alloys with high strength

Not only plasticity at RT, but also the strength of low-alloyed Mg alloys need to be further improved. GB segregation can also be used to regulate or improve the strength of Mg alloys, and the impact is generally divided into two aspects. (a) GB segregation shows certain dragging effect on the dislocation motion, results in a positive deviation of k value and an additional strengthening [162–164]. Bobylev et al. [165] proposed a model explaining enhanced strength of ultrafine-grained alloys containing GB segregation. The τseg can be estimated based on the growing rectangular glide dislocation loop as the formula [163,165–167]:

$$\tau_{\text{seg}} = \frac{2}{Lh} \max_{-L/2<x_1<L/2} \int_0^h dx_3 \int_{-L/2}^0 \sigma_{23}(x_1, x_2, x_3) dx_2 \qquad (15)$$

where L is the effective distance between the centers of neighboring segregated atoms, h is the distance that the dislocation loop grows in the direction parallel to the GB plane, and σ_{23} is the segregation stress. However, compared with metals such as Cu and Fe, the hindrance effect of GB segregation in Mg alloys is often smaller [159,160], indicating that the direct increase in YS caused by such effect is very limited.

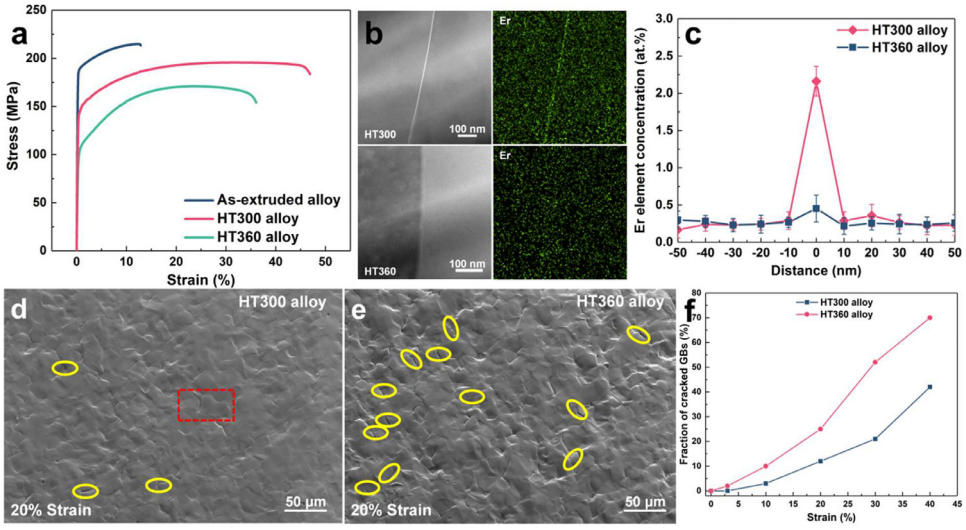

Fig. 11. (a) Stress-strain curves, (b,c) GB segregation, and (d–f) GB cracking observation of Mg-2Er alloys [12]. (Reprinted from Int. J. Plasticity 162, Developing a Mg alloy with ultrahigh room temperature ductility via grain boundary segregation and activation of non-basal slips, 103,548, Copyright 2023, with permission from Elsevier.)

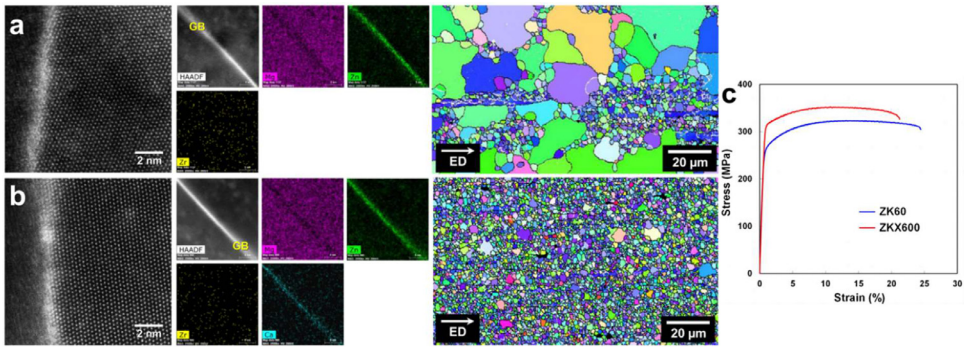

Fig. 12. GB segregation and grain structure of (a) ZK60 and (b) ZKX600 alloys. (c) Stress-strain curves of ZK60 and ZKX600 alloys [170]. (Reprinted from Scripta Mater. 187, Factors affecting the grain refinement of extruded Mg-6Zn-0.5Zr alloy by Ca addition, 26,28, Copyright 2020, with permission from Elsevier.)

This is because it is difficult for Mg alloys to form ultra-fine grains, and dislocation accumulation would significantly reduce the strengthening caused by GB segregation [165]. For example, Pan et al. [5,13] attributed the difference between the predicted and experimental YS values to the hindering effect of GB segregation on dislocations. Overall, the incremental contribution caused by the hindrance of GB segregation cannot currently be accurately assessed and is relatively small. This has also led to the fact that GB segregation of Mg alloys is almost not considered when evaluating strengthening increment. (b) The excellent effect of GB segregation on strength is mainly reflected in refining grains and inhibiting grain growth during the thermal processing or annealing process [168,169]. Based on the Hall-Petch relationship [28,30], YS (σ_{ys}) is inversely proportional to average grain size:

$$\sigma_{ys} = \sigma_0 + kd^{-1/2} \tag{16}$$

where σ_0 is the friction stress, k is the locking parameter, and d is the average grain size. The k values of Mg alloys are mainly between 200 MPa$(\mu m)^{1/2}$ and 300 MPa$(\mu m)^{1/2}$, which is obviously higher than those of pure Al and Al alloys [30]. In other words, grain refinement can effectively improve the yield strength of Mg alloys, indicating the significance of refining grains or controlling grain growth in Mg alloys. Kim et al. [170] compared the GB segregation, grain structure and mechanical properties of Mg-6Zn-0.5Zr (wt%, ZK60) and Mg-6Zn-0.5Zr-0.2Ca (wt%, ZKX600) alloys, and found that the strong Zn and Ca GB co-segregation results in finer grains of ZKX600 alloy than that of ZK60 alloy (ZKX60 alloy: 1.6 μm; ZK60 alloy: 4.2 μm) under the extrusion temperature of 250 °C. The YS increment caused by grain refinement from 4.2 μm to 1.6 μm is about 67 MPa, which is very close to experimental increment (Fig. 12). In our previous study [68], it was also found that the high segregation level would be conducive to obtaining fine grains in the ZXM-Sm alloy during annealing, leading to a higher YS (Fig. 13).

GB segregation can significantly improve the stability of fine grains and inhibit grain growth. Xiao et al. [46–48] introduced ultra-fine grains with an average grain size of ~100 nm to the Mg-2.57Ag (wt%) alloy by cold rolling and subsequent annealing. This is because Ag clusters and segregation promote the formation of noncrystalline and inhibit their growth during the annealing process. Our team [68] systematically studied the relationship between the GB segregation level and the grain size during annealing in Mg-Zn-Mn-Ca and Mg-Zn-Mn-Ca-Sm alloys (Fig. 14). The two as-extruded alloys exhibit consistently similar grain sizes and grain distribution, indicating a similar driving force for grain growth. After annealing, these two alloys show significantly different grain growth rates, i.e., the Mg-Zn-Mn-Ca alloy has greater growth rate (Fig. 14). The Mg-Zn-Mn-Ca-Sm alloys show higher segregation level than the Mg-Zn-Mn-Ca alloys due to the Zn/Ca/Sm co-segregation, and correspondingly, its suppression effect of grain growth is significantly better than that of the Sm-free alloys during annealing (Fig. 14). Qian et al. [158] found that micro Ca addition would increase the Zn and Ca segregation level of GB in Mg-Zn-Ce alloy, and the as-extruded Ca-containing alloys obtains finer grains than as-extruded Mg-Zn-Ce alloys.

The strength-plasticity trade-off is prevalent in metallic materials. The coordination of strength and plasticity is often difficult to achieve directly through simple processing, which has extremely high requirements on the process. Take hot extrusion as an example, lower extrusion temperatures tend to correspond to obtain low fraction of recrystallized grains and high dislocation density, leading to high strength and low plasticity [171–174]. On the contrary, high extrusion temperatures often lead to high ductility and low strength. It's easy to think of a common way for designing the low-alloyed Mg alloys with high strength-plasticity by low-temperature extrusion and subsequent annealing. However, the rapid growth of grains during the annealing process would lead to a significant decrease in strength, which is a potential problem with this method. In other words, if we could inhabit grain growth during annealing process, an effective strategy for developing high-strength and high-plasticity Mg alloys can be proposed. Based on the above analysis, we proposed an effective strategy for designing low-alloyed Mg alloys with high strength-plasticity via inhibiting grain growth through introducing strong GB segregation. Following this strategy, our team [14] has successfully developed a new low-alloyed Mg-2Sm-0.8Mn-0.6Ca-0.5Zn (wt%) alloy with high strength-

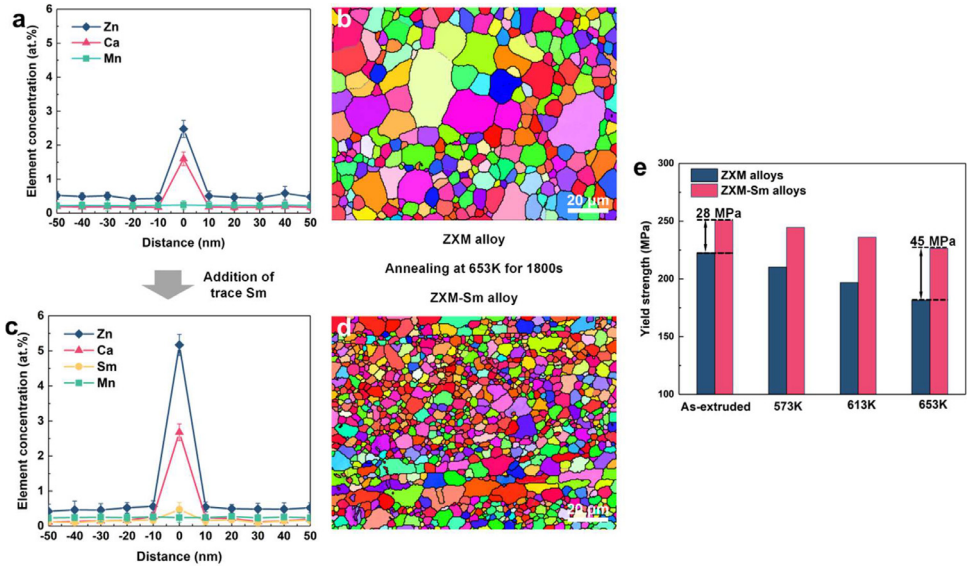

Fig. 13. GB segregation and grain structure of (a,b) Mg-Zn-Mn-Ca (ZXM) and (c,d) Mg-Zn-Mn-Ca-Sm (ZXM-Sm) alloys [68]. (e) YS of these two alloys with different states. (Reprinted from Mater. Sci. Eng. A 831, Significantly enhanced grain boundary Zn and Ca co-segregation of dilute Mg alloy via trace Sm addition, 142,259, Copyright 2022, with permission from Elsevier.)

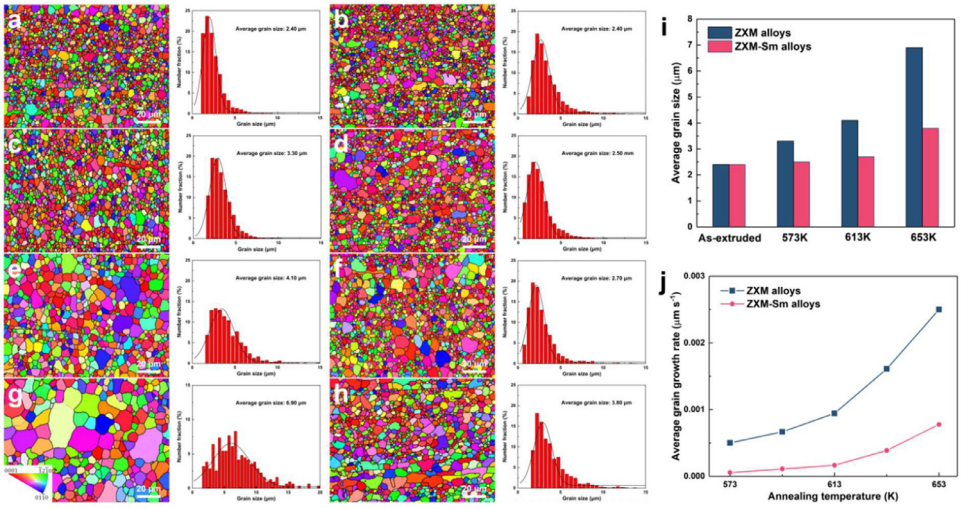

Fig. 14. Grain structure and size distribution of (a,c,e,g) ZXM and (b,d,f,h) ZXM-Sm alloys: (a,b) as-extruded state; (c,d) annealing at 573 K (300 °C); (e,f) annealing at 613 K (340 °C); (g,h) annealing at 653 K (380 °C). (i) Average grain size and (j) grain growth rate of these two alloys annealed with different temperatures [68]. (Reprinted from Mater. Sci. Eng. A 831, Significantly enhanced grain boundary Zn and Ca co-segregation of dilute Mg alloy via trace Sm addition, 142,259, Copyright 2022, with permission from Elsevier.)

ductility via low-temperature extrusion and subsequent annealing (Fig. 15). The as-extruded alloy with bimodal grain structure and high-density dislocations exhibits high strength (YS: 453 MPa) and low elongation (3.2%). During annealing, high level of Zn/Ca/Sm GB co-segregation inhibits the movement of high-angle GBs, while segregation-free dislocations and low-angle GBs would annihilate rapidly. Eventually, the Mg alloy after properly annealing exhibits a completely fine-grained structure (average grain size: 1.9 μm), obtaining high strength (YS: 403 MPa) and high elongation (15.5%).

The Fig. 16 shows the strength and elongation of some reported high mechanical performance low-alloyed Mg alloys. The area marked in red is the high-strength low-alloyed Mg alloys containing obvious GB segregation, and the yellow area is the high-plasticity low-alloyed Mg alloys containing significant GB segregation. It can be seen that if the GB segregation strategy can be rationally utilized, it is expected to successfully design high-strength/high-plasticity low-alloyed Mg alloys. The overall YS of high-strength Mg alloys developed by GB segregation strategy is mostly higher than 300 MPa, and the elongation is mostly greater than 5%, which could meet the most application needs. For high-plasticity Mg alloys designed by GB segregation strategies, the elongation can mostly exceed 30%.

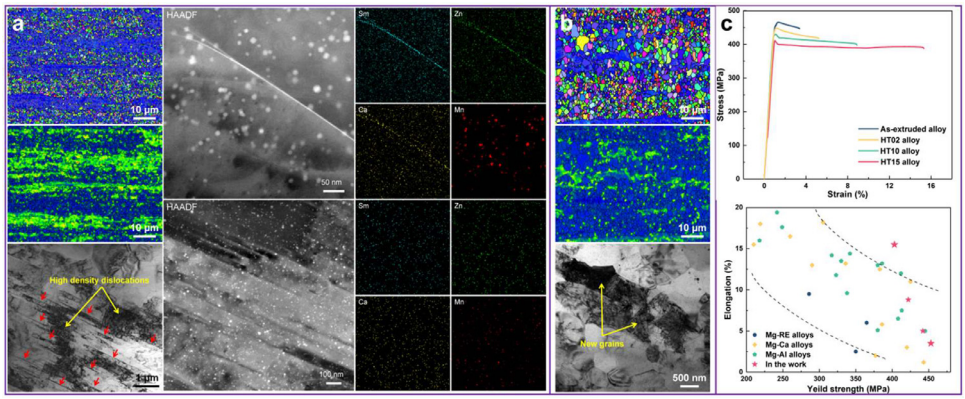

Fig. 15. Microstructure of Mg-2Sm-0.8Mn-0.6Ca-0.5Zn alloys (a) before and (b) after annealing at 350 °C for 15 min. (c) Mechanical properties of Mg-2Sm-0.8Mn-0.6Ca-0.5Zn alloys and other reported alloys [14]. (Reprinted from Scripta Mater. 209, Developing a low-alloyed fine-grained Mg alloy with high strength-ductility based on dislocation evolution and grain boundary segregation, 114,414, Copyright 2022, with permission from Elsevier.)

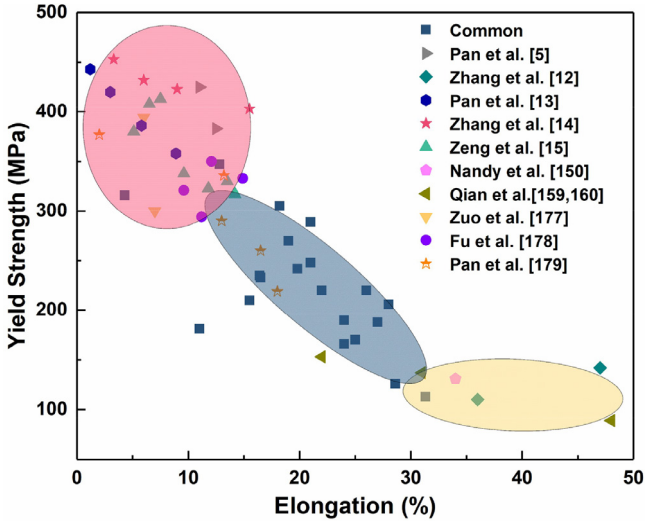

Fig. 16. Scatter plot of strength vs. elongation of some reported high mechanical performance low-alloyed Mg alloys [5,12–15,148,157,158,175–187].

5. GB segregation strategy for designing low-alloyed Mg alloys with high formability

Numerous efforts and attempts have been made in the past few years to overcome the bottleneck of low formability in Mg alloys. GB segregation is an effective strategy for improving the formability of Mg alloys at RT. On the one hand, traditional Mg alloys are prone to develop strong basal texture during deformation (especially rolled or extruded sheets), which makes it difficult to adapt to deformation along the thickness direction, leading to a poor RT formability. GB segregation can effectively weaken basal texture and/or change basal texture characteristics during thermal processing and heat treatment, improving the formability at RT. For example, Trang et al. [65] proposed an alloy design concept for high-strength and high-formability Mg alloys, in which some alloying elements are used to achieve precipitation strengthening while the other elements maximize GB segregation to regulate the texture. They developed a new Mg-3Al-1Zn-1Mn-0.5Ca (wt%) alloy with high Zn/Ca GB co-segregation level by twin-roll casting process, showing weakened and splitted basal texture along rolling direction. The co-segregation of Zn and Ca decreases GB energy and induces GB pinning effect during recrystallization and grain growth, thereby reducing the GB mobility and inhibiting grain growth into preferable orientation (i.e., basal texture orientation). This newly developed alloy presents a high formability with Index Erichsen (I.E.) value of 8 mm, accompanied by a high YS of 219 MPa. Nakata et al. [188–191] reported the effect of GB segregation on basal texture and formability of the AZ31 alloys, and found that the Mg alloy with stronger GB segregation of Al and Zn has a weakened split-texture along rolling direction, improving the I.E. values from 3 mm to 6.6 mm. Bian et al. [93] introduced trace Cu and Ca elements into pure Mg to form Cu and Ca GB co-segregation, weakening basal texture from 19.3 multiples of random distribution (mrd) to 3.1 mrd and remarkably improving I.E. values from 2.9 mm to 7.7 mm (Fig. 17). Bian et al. [192] also proposed an effective method for weakening basal texture by Zn GB segregation and high-temperature final rolling process, activating more pyramidal $<c + a>$ slips and improving I.E. values from 4.1 mm to 7.9 mm.

On the other hand, introducing non-uniform/heterogeneous grains into Mg alloys via GB segregation is also an effective method to improve the formability at RT. Kang et al. [193] systematically studied the relationship between formability and work hardening capacity/elongation, and found that high formability at RT is highly consistent with large work hardening capacity and high elongation. In other words, the methods that could simultaneously increase work hardening and elongation have great potential to be used to optimize formability at RT. Non-uniform/heterogeneous grains/structure would produce the local strain, increasing back stress and work hardening [136,194–196], and meanwhile, back stress would activate more non-basal slips and improve the elongation of failure at RT [194]. As mentioned by Section 2.2, GB segregation can contribute to the forma-

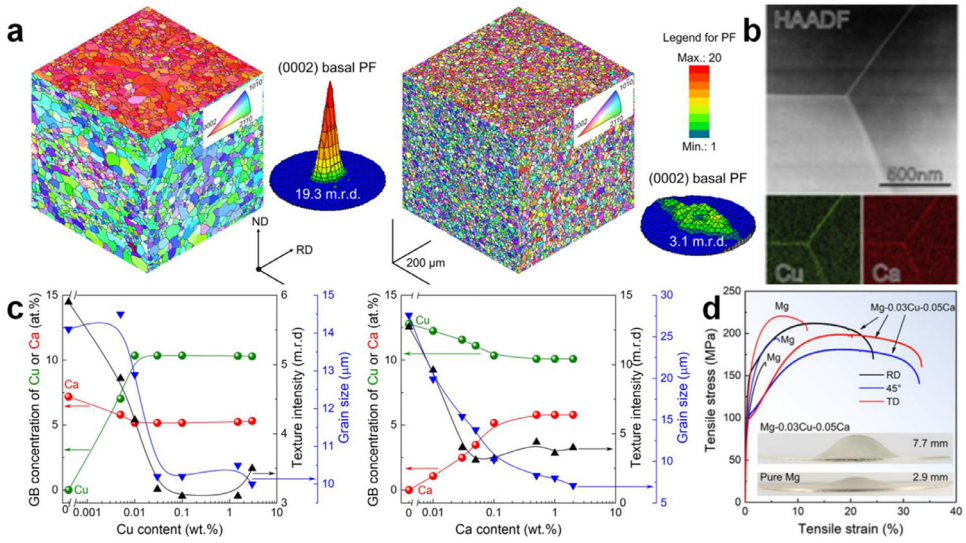

Fig. 17. (a) Grain structure + basal texture and (b) GB segregation of pure Mg and Mg-0.03Cu-0.05Ca (wt%) alloy. (c) Correlation between the GB concentration of Cu or Ca, grain size, and texture intensity of Mg-xCu-0.1Ca (wt%) and Mg-0.03Cu-yCa (wt%) alloys. (d) Properties of pure Mg and Mg-0.03Cu-0.05Ca (wt%) alloy [93]. (Reprinted from Acta Mater., 241, Improving the mechanical and corrosion properties of pure magnesium by parts-per-million-level alloying, 118,393, Copyright 2022, with permission from Elsevier.)

tion of weakly textured heterogeneous grains under certain circumstances (such as high-temperature annealing and thermal deformation processes). In this cases, some GBs with sufficient velocity (such as some GBs with relatively low segregation level or GBs of grains with initial large size) first break away from drag caused by segregation [98,99,197], which is conducive to formation of larger grains. Other GBs are still loaded with developing solute atmosphere. During curvature driven grain growth, these larger grains with supercritical driving force would be able to overcome solute pinning and exhibit rapid free growth [197–199], leading to the formation of a heterogeneous-grained structure.

From the above two aspects, it can be inferred that rational use of GB segregation to promote the formation of both two microstructural features, i.e. weakened texture and heterogeneous structure, is expected to efficiently improve the formability at RT. Based on the strategy, Our team [200] successfully designed a new Mg-Sm alloy with high Zn/Sm/Ca grain co-segregation, obtaining weakened-textured heterogeneous grains via high-temperature annealing process. The developed alloy shows high elongation and large work hardening capacity, indicating a high formability at RT.

6. Summary and outlook

GB segregation is an effective strategy for preparing high mechanical performance low-alloyed Mg alloys, which can help to make up for the disadvantages such as low strength, poor plasticity and unsatisfactory formability at RT to a certain extent. The specific summary and outlook are as follows:

(1) The sites of the segregation atoms are related to the atomic radius and electronegativity. The “large’’ atoms tend to occupy the “extension position’’, while the “small’’ atoms tend to occupy the “contraction position’’. Solute atoms with higher electronegativity than Mg tend to occupy “contraction position’’, while solute atoms with lower electronegativity than Mg tend to occupy “extension position’’ positions. However, current research is mainly focused on coherent interfaces (such as TB), and there are few such studies on incoherent interface segregation behavior as well as multi-element co-segregation behavior.

(2) Since GBs are incoherent interfaces and have high complexity, GB segregation behavior is general more complicated, and there are currently relatively few relevant simulations and atomic scale evidence. It is precisely because of the complex structural characteristics that it is possible to improve the level of GB segregation and optimize the segregation behavior.

(3) GB segregation could increase GB cohesion and help activate non-basal slip to a certain extent, ultimately improving plasticity of Mg alloys at RT. There have been studies on GB segregation-induced embrittlement in other metals, but there are few related reports on Mg alloys. Whether the characteristic and content of segregation have adverse effects on the plasticity of Mg alloys remains to be further studied.

(4) GB segregation can inhibit grain growth during thermal deformation or annealing, which is beneficial to obtaining a fine-grained structure. For low-alloyed Mg alloys with strong GB segregation, fine-grained structure and dislocation density/structure can be controlled by annealing and other processes to obtain both high strength and high plasticity.

(5) Introduction of heterogeneous grains with weakened texture through GB segregation is expected to efficiently improve the formability of Mg alloys. On the one hand,

the weakening of the basal texture caused by GB segregation can reduce the plastic anisotropy, on the other hand, heterogeneous grains, formed by controlling grain growth due to GB segregation, would lead to large working hardening capacity and high elongation.

Declaration of competing interest

R. Wu is an editorial board member for Journal of Magnesium and Alloys and was not involved in the editorial review or the decision to publish this article. All authors declare that there are no competing interests.

CRediT authorship contribution statement

Zhi Zhang: Writing – review & editing, Writing – original draft, Data curation. **Jinshu Xie:** Data curation, Writing – review & editing. **Jinghuai Zhang:** Funding acquisition, Supervision, Writing – review & editing. **Xu-Sheng Yang:** Funding acquisition, Supervision, Writing – review & editing. **Ruizhi Wu:** Conceptualization, Supervision.

Acknowledgements

The authors acknowledge gratefully the support of the National Natural Science Foundation of China (52071093 and 51871069), the Natural Science Foundation of Heilongjiang Province of China (LH2023E059), the Fundamental Research Program of Shenzhen Science and Technology Innovation Commission (JCYJ20210324131405015) and PolyU Grant (1-BBR1).

References

[1] Y. Yang, X.M. Xiong, J. Chen, X.D. Peng, D.L. Chen, F.S. Pan, J. Magnes. Alloy. 9 (2021) 705–747.
[2] J.S. Xie, J.H. Zhang, Z.H. You, S.J. Liu, K. Guan, R.Z. Wu, J. Wang, J. Feng, J. Magnes. Alloy. 9 (2021) 41–56.
[3] Y. Yang, X.M. Xiong, J. Chen, X.D. Peng, D.L. Chen, F.S. Pan, J. Magnes. Alloy. 11 (2023) 2611–2654.
[4] J.H. Zhang, S.J. Liu, R.Z. Wu, L.G. Hou, M.L. Zhang, J. Magnes. Alloy. 6 (2018) 277–291.
[5] H.C. Pan, R. Kang, J.R. Li, H.B. Xie, Z.R. Zeng, Q.Y. Huang, C.L. Yang, Y.P. Ren, G.W. Qin, Acta Mater. 186 (2020) 278–290.
[6] J.Y. Zhang, J.S. Miao, N. Balasubramani, D.H. Cho, T. Avey, C.Y. Chang, A.A. Luo, J. Magnes. Alloy. 11 (2023) 3867–3895.
[7] T.S. Wang, Z.M. Hua, C. Wang, M. Zha, Y.P. Gao, H.Y. Wang, J. Magnes. Alloy. (2023) Accept, doi:10.1016/j.jma.2023.05.014.
[8] W.Q. Xu, N. Birbilis, G. Sha, Y. Wang, J.E. Daniels, Y. Xiao, M. Ferry, Nat. Mater. 14 (2015) 1229–1235.
[9] Q.C. Zhu, Y.X. Li, F.Y. Cao, D. Qiu, Y. Yang, J.Y. Wang, H. Zhang, T. Ying, W.J. Ding, X.Q. Zeng, Nat. Commun. 13 (2022) 5838.
[10] G.G. Wang, J.P. Weiler, J. Magnes. Alloy. 11 (2023) 78–87.
[11] X. Luo, Z.Q. Feng, T.B. Yu, J.Q. Luo, T.L. Huang, G.L. Wu, N. Hansen, X.X. Huang, Acta Mater. 183 (2020) 398–407.
[12] Z. Zhang, J.H. Zhang, J.S. Xie, S.J. Liu, W. Fu, R.Z. Wu, Int. J. Plast. 162 (2023) 103548.
[13] H.C. Pan, G.W. Qin, Y.M. Huang, Y.P. Ren, X.C. Sha, X.D. Han, Z.Q. Liu, C.F. Li, X.L. Wu, H.W. Chen, C. He, L.J. Chai, Y.Z. Wang, J.F. Nie, Acta Mater. 149 (2018) 350–363.
[14] Z. Zhang, J.H. Zhang, J.S. Xie, S.J. Liu, Y.Y. He, K. Guan, R.Z. Wu, Scr. Mater. 209 (2022) 114414.
[15] Z.R. Zeng, Y.M. Zhu, J.F. Nie, S.W. Xu, C.H.J. Davies, N. Birbilis, Metall. Mater. Trans. A 50A (2019) 4344–4363.
[16] X.Q. Liu, X.G. Qiao, R.S. Pei, Y.Q. Chi, L. Yuan, M.Y. Zheng, J. Magnes. Alloy. 11 (2023) 553–561.
[17] Y.C. Wan, B. Tang, Y.H. Gao, L.L. Tang, G. Sha, B. Zhang, N.N. Liang, C.M. Liu, S.N. Jiang, Z.Y. Chen, X.Y. Guo, Y.H. Zhao, Acta Mater. 200 (2020) 274–286.
[18] J.S. Ji, J. Zheng, L.C. Jia, Y. Zhang, Y.F. Jia, Y.S. Shi, H. Zhang, Y. Xue, J. Magnes. Alloy. 11 (2023) 3382–3393.
[19] M.Z. Bian, T.T. Sasaki, T. Nakata, Y. Yoshida, N. Kawabe, S. Kamado, K. Hono, Acta Mater. 158 (2018) 278–288.
[20] R.X. Zheng, J.P. Du, S. Gao, H. Somekawa, S. Ogata, N. Tsuji, Acta Mater. 198 (2020) 35–46.
[21] Z.R. Zeng, M.R. Zhou, P. Lynch, F. Mompiou, Q.F. Gu, M. Esmaily, Y.M. Yan, Y. Qiu, S.W. Xu, H. Fujii, C. Davies, J.F. Nie, N. Birbilis, Acta Mater. 206 (2021) 116648.
[22] Z.R. Zeng, J.F. Nie, S.W. Xu, C.H.J. Davies, N. Birbilis, Nat. Commun. 8 (2017) 972.
[23] H.Y. Wang, Z.P. Yu, L. Zhang, C.G. Liu, M. Zha, C. Wang, Q.C. Jiang, Sci. Rep. 5 (2015) 17100.
[24] Y.T. Zhu, X.L. Wu, Prog. Mater. Sci. 131 (2023) 101019.
[25] G.H. Wu, X. Tong, C. Wang, R. Jiang, W.J. Ding, J. Magnes. Alloy. 11 (2023) 3463–3483.
[26] A. Rezaei, R. Mahmudi, R.E. Logé, J. Magnes. Alloy. 11 (2023) 3815–3828.
[27] Q. Zeng, Y.B. Zhang, K.M. Li, Y. Zhuang, J.H. Li, Y.J. Yuan, D.D. Yin, J. Magnes. Alloy. 11 (2023) 533–542.
[28] E.O. Hall, Proc. Phys. Soc. Lond. Sect. B 64 (1951) 747–753.
[29] N. Hansen, Scr. Mater. 51 (2004) 801–806.
[30] Z. Zhang, J.H. Zhang, J. Wang, Z.H. Li, J.S. Xie, S.J. Liu, K. Guan, R.Z. Wu, Int. J. Miner. Metall. Mater. 28 (2021) 30–45.
[31] S.M. Razavi, D.C. Foley, I. Karaman, K.T. Hartwig, O. Duygulu, L.J. Kecskes, S.N. Mathaudhu, V.H. Hammond, Scr. Mater. 67 (2012) 439–442.
[32] B.B. Wang, G.M. Xie, L.H. Wu, P. Xue, D.R. Ni, B.L. Xiao, Y.D. Liu, Z.Y. Ma, Mater. Sci. Eng. A 820 (2021) 141504.
[33] T. Wang, M. Zha, Y.P. Gao, S.Q. Wang, H.L. Jia, C. Wang, H.Y. Wang, Int. J. Plast. (2023) 103766.
[34] S.S. Liu, D.B. Xia, H. Yang, G.S. Huang, F.X. Yang, X.H. Chen, A.T. Tang, B. Jiang, F.S. Pan, Int. J. Plast. 157 (2022) 103371.
[35] M. Zha, S.Q. Wang, T. Wang, H.L. Jia, Y.K. Li, Z.M. Hua, K. Guan, C. Wang, H.Y. Wang, Mater. Res. Lett. 11 (2023) 772–780.
[36] Y.K. Li, M. Zha, H.L. Jia, S.Q. Wang, H.M. Zhang, X. Ma, T. Tian, P.K. Ma, H.Y. Wang, J. Magnes. Alloy. 9 (2021) 1556–1566.
[37] Z.Z. Jin, M. Zha, S.Q. Wang, S.C. Wang, C. Wang, H.L. Jia, H.Y. Wang, J. Magnes. Alloy. 10 (2022) 1191–1206.
[38] P. Luo, D.T. McDonald, W. Xu, S. Palanisamy, M.S. Dargusch, K. Xia, Scr. Mater. 66 (2012) 785–788.
[39] L. Zhang, Z.H. Zhang, X. Zhang, X.X. Huang, J. Mater. Res. Technol. 21 (2022) 161–185.
[40] C. He, Z.Q. Li, H.W. Chen, N. Wilson, J.F. Nie, Nat. Commun. 12 (2021) 722.
[41] H.B. Xie, H.C. Pan, J.Y. Bai, D.S. Xie, P.J. Yang, S.S. Li, J.F. Jin, Q.Y. Huang, Y.P. Ren, G.W. Qin, Nano Lett. 21 (2021) 9642–9650.
[42] K. Lu, L. Lu, S. Suresh, Science 324 (2009) 349.
[43] Z. Yu, P.R. Cantwell, Q. Gao, D. Yin, Y. Zhang, N. Zhou, G.S. Rohrer, M. Widom, J. Luo, M.P. Harmer, Science 358 (2017) 97–101.
[44] J.F. Nie, Y.M. Zhu, J.Z. Liu, X.Y. Fang, Science 340 (2013) 957–960.
[45] X.Y. Shi, Y. Liu, J. Lu, R.E.A. Williams, D.J. Li, X.Q. Zeng, A.A. Luo, Scr. Mater. 112 (2016) 136–139.
[46] L.R. Xiao, X.F. Chen, K. Wei, Y. Liu, D.D. Yin, Z.H. Hu, H. Zhou, Y.T. Zhu, Scr. Mater. 191 (2021) 219–224.
[47] L.R. Xiao, X.F. Chen, Y. Cao, H. Zhou, X.L. Ma, D.D. Yin, B. Ye, X.D. Han, Y.T. Zhu, Scr. Mater. 177 (2020) 69–73.
[48] L.R. Xiao, X.F. Chen, H.Y. Ning, P. Jiang, Y. Liu, B. Chen, D.D. Yin, H. Zhou, Y.T. Zhu, J. Magnes. Alloy. 10 (2022) 2510–2515.
[49] X. Wang, Y. Hu, K.H. Yu, S. Mahajan, I.J. Beyerlein, E.J. Lavernia, T.J. Rupert, J.M. Schoenung, Scr. Mater. 209 (2022) 114375.

[50] H. Zhou, W.Z. Xu, W.W. Jian, G.M. Cheng, X.L. Ma, W. Guo, S.N. Mathaudhu, Q.D. Wang, Y.T. Zhu, Philos. Mag. 94 (2014) 2403–2409.
[51] J. Zhang, Y.C. Dou, Y. Zheng, Scr. Mater. 80 (2014) 17–20.
[52] S.L. Shang, W.Y. Wang, B.C. Zhou, Y. Wang, K.A. Darling, L.J. Kecskes, S.N. Mathaudhu, Z.K. Liu, Acta Mater. 67 (2014) 168–180.
[53] H. Ju, H. Ning, Z.Y. Meng, C. Wang, H.Y. Wang, J. Mater. Res. Technol. 24 (2023) 8558–8571.
[54] Z.R. Zeng, Y.M. Zhu, S.W. Xu, M.Z. Bian, C.H.J. Davies, N. Birbilis, J.F. Nie, Acta Mater. 105 (2016) 479–494.
[55] H.S. Jang, D. Seol, B.J. Lee, J Alloy. Compd. 894 (2022) 162539.
[56] R.S. Pei, Z.C. Xie, S.B. Yi, S. Korte-Kerzel, J. Guénolé, T. Al-Samman, Scr. Mater. 230 (2023) 115432.
[57] X.H. Shao, Z.Z. Peng, Q.Q. Jin, X.L. Ma, Acta Mater. 118 (2016) 177–186.
[58] J.F. Nie, K. Oh-Ishi, X. Gao, K. Hono, Acta Mater. 56 (2008) 6061–6076.
[59] X.J. Zhao, H.W. Chen, N. Wilson, Q. Liu, J.F. Nie, Nat. Commun. 10 (2019) 3243.
[60] H. Zhou, G.M. Cheng, X.L. Ma, W.Z. Xu, S.N. Mathaudhu, Q.D. Wang, Y.T. Zhu, Acta Mater. 95 (2015) 22–29.
[61] H.R. Wu, J.H. Jiang, Z.Q. Yang, M.J. Li, H. Huang, N.F. Ge, A.B. Ma, H. Liu, J. Magnes. Alloy. 11 (2023) 3765–3778.
[62] H.B. Xie, Q.Y. Huang, J.Y. Bai, S.S. Li, Y. Liu, J.G. Feng, Y.S. Yang, H.C. Pan, H.X. Li, Y.P. Ren, G.W. Qin, Nano Lett. 21 (2021) 2870–2875.
[63] D.K. Guan, X.G. Liu, J.H. Gao, L. Ma, B.P. Wynne, W.M. Rainforth, Sci. Rep. 9 (2019) 7152.
[64] L.Y. Zhao, H. Yan, R.S. Chen, E.H. Han, J. Magnes. Alloy. 9 (2021) 818–828.
[65] T.T.T. Trang, J.H. Zhang, J.H. Kim, A. Zargaran, J.H. Hwang, B.C. Suh, N.J. Kim, Nat. Commun. 9 (2018) 2522.
[66] Z.M. Hua, B.Y. Wang, C. Wang, H.M. Zhang, C.F. Du, Y.J. Li, M. Zha, P.K. Ma, Z.Z. Yang, H.Y. Wang, Materialia 14 (2020) 100918.
[67] R.S. Pei, Y.C. Zou, D.Q. Wei, T.A. Samman, Acta Mater. 208 (2021) 116749.
[68] Z. Zhang, J.S.Xie J.H. Zhang, S.J. Liu, Y.Y. He, R. Wang, D.Q. Fang, W. Fu, Y.L. Jiao, R.Z. Wu, Mater. Sci. Eng. A 831 (2022) 142259.
[69] S.K. Woo, R.S. Pei, T. Al-Samman, D. Letzig, S.B. Yi, J. Magnes. Alloy. 11 (2023) 543–552.
[70] R.S. Pei, Y.J. Zhaoa, M. Zubair, S.B. Yi, T. Al-Samman, J. Magnes. Alloy. 11 (2023) 2312–2325.
[71] T.T. Sasaki, J.Y. Lin, P. Yi, Z.H. Li, S.E. Prameela, A. Park, E. Lipkin, A. Lee, M.L. Falk, T.P. Weihs, K. Hono, Scr. Mater. 220 (2022) 114924.
[72] Y.C. Lai, Y. Ying, D. Yadav, J. Guerrero, Y.J. Hu, K.Y. Xie, J. Magnes. Alloy. 11 (2023) 4513–4524.
[73] Y.J. Hu, V. Menon, L. Qi, J. Magnes. Alloy. 10 (2022) 2717–2729.
[74] L.K. Bao, P. Du, S.K. Xi, C.P. Wang, K.H. Zheng, R.P. Shi, G.Q. Xie, X.J. Liu, J. Magnes. Alloy. (2023), doi:10.1016/j.jma.2022.12.010.
[75] V. Menon, S. Das, V. Gavini, L. Qi, Acta Mater. 264 (2024) 119515.
[76] X.K. Zhang, J. Yan, Y.H. Chen, R. Kevorkyants, T.Q. Wen, X. Sun, A. Hu, J.C. Huang, Int. J. Plast. 166 (2023) 103643.
[77] Y. Yang, F. Liu, K.F. Chen, B.Y. Liu, Z.W. Shan, B. Li, J. Magnes. Alloy. 11 (2023) 4498–4512.
[78] R.K. Koju, Y. Mishin, Acta Mater. 201 (2020) 596–603.
[79] P. Lejcek, Grain Boundary Segregation in Metals, Springer, 2010.
[80] J.N. Zhang, Y. Jiang, Z.Q. Liu, Y.R. Wang, Surf. Interfaces 41 (2023) 103235.
[81] W.T. Sun, Y. He, X.G. Qiao, X.J. Zhao, H.W. Chen, N. Gao, M.J. Starink, M.Y. Zheng, J. Magnes. Alloy. 11 (2023) 4589–4602.
[82] W. Xu, B. Zhang, K. Du, X.Y. Li, K. Lu, Acta Mater. 226 (2022) 117640.
[83] M. Guttmann, D. McLean, Interficial Segregation in: W.C. Johnson, J.M. Blakely (Eds.), ASM, Metals Park, 1979.
[84] R.H. Fowler, E.A. Guggenheim, Statistical Thermodynamics, Macmillan, New York, 1939.
[85] N.X. Zhou, T. Hu, J. Luo, Curr. Opin. Solid State Mater. Sci. 20 (2016) 268–277.
[86] M. Guttmann, in: Atomistics of Fracture, Plenum Press, New York, 1983, pp. 465–491. ed. by R.M. Latanision, J.R. Pickens.
[87] M. Guttmann, P.R. Krahe, F. Abel, G. Amsel, M. Bruneaux, C. Cohen, Metall. Trans. 5 (1974) 167–177.
[88] P. Gas, M. Guttmann, J. Bernardini, Acta Metall. 30 (1982) 1309–1316.
[89] H.J. Grabke, K. Hennesen, R. Möller, W. Wei, Scr. Metall. 21 (1987) 1329–1334.
[90] C.L. Briant, Scr. Metall. 15 (1981) 1013–1018.
[91] D.Y. Lee, E.V. Barrera, J.P. Stark, H.L. Marcus, Metall. Trans. A 15 (1984) 1415–1430.
[92] C.L. Briant, A.M. Ritter, Acta Metall. 32 (1984) 2031–2042.
[93] M.Z. Bian, I. Nakatsugawa, Y. Matsuoka, X.S. Huang, Y. Tsukada, T. Koyama, Y. Chino, Acta Mater. 241 (2022) 118393.
[94] F. Mouhib, R. Pei, B. Erol, F. Sheng, S. Korte-Kerzel, T. Al-Samman, Mater. Sci. Eng. A 847 (2022) 143348.
[95] X.J. Luo, H. Yang, J.X. Zhou, B. Jiang, Q.G. Feng, Y. Zeng, W. Li, Z.H. Dong, J.F. Song, J.Y. Xu, G.S. Huang, D.F. Zhang, F.S. Pan, Scr. Mater. 236 (2023) 115672.
[96] Z.X. Yan, Q. Yang, F.Z. Meng, R. Ma, R.R. Bao, X.J. Liu, J. Meng, X. Qiu, J. Mater. Sci. Technol. 93 (2021) 103–109.
[97] F. Christien, R.Le Gall, G. Saindrenan, Acta Mater. 51 (2003) 521–534.
[98] J.W. Cahn, Acta Metall. 10 (1962) 789–798.
[99] K. Lücke, H.P. Stüwe, Acta Metall. 19 (1971) 1087–1099.
[100] M.M. Hoseini-Athar, R. Mahmudi, R. Prasath Babu, P. Hedström, J. Alloys Compd. 806 (2019) 1200–1206.
[101] M.M. Hoseini-Athar, R. Mahmudi, Mater. Sci. Eng. A 759 (2019) 745–753.
[102] M.M. Hoseini-Athar, R. Mahmudi, R. Prasath Babu, P. Hedström, Mater. Sci. Eng. A 754 (2019) 390–399.
[103] I.H. Jung, M. Sanjari, J. Kim, S. Yue, Scr. Mater. 102 (2015) 1–6.
[104] S.K. Das, Y.B. Kang, T. Ha, I. Jung, Acta Mater. 71 (2014) 164–175.
[105] J.D. Robson, S.J. Haigh, B. Davis, D. Griffiths, Metall. Mater. Trans. A 47 (2016) 522–530.
[106] S.A. Farzadfar, E. Martin, M. Sanjari, E. Essadiqi, S. Yue, J. Mater. Sci. 47 (2012) 5488–5500.
[107] M. Sanjari, A. Farzadfar, A.S.H. Kabir, H. Utsunomiya, I.H. Jung, R. Petrov, L. Kestens, S. Yue, J. Mater. Sci. 49 (2014) 1408–1425.
[108] X. Li, P. Yang, L.N. Wang, L. Meng, F. Cui, Mater. Sci. Eng. A 517 (2009) 160–169.
[109] T. Al-Samman, G. Gottstein, Mater. Sci. Eng. A 490 (2008) 411–420.
[110] G.H. Huang, D.D. Yin, J.W. Lu, H. Zhou, Y. Zeng, G.F. Quan, Q.D. Wang, Mater. Sci. Eng. A 720 (2018) 24–35.
[111] C.J. Silva, A. Kula, R.K. Mishra, M. Niewczas, J. Alloy. Compd. 687 (2016) 548–561.
[112] M. Sanjari, A.R. Farkoosh, B. Shalchi Amirkhiz, Y. He, A. Javaid, A.S. Kabir, J. Su, I.H. Jung, S. Yue, Scr. Mater. 134 (2017) 1–5.
[113] M. Bugnet, M. Niewczas, A. Kula, G.A. Botton, Acta Mater. 79 (2014) 66–73.
[114] M.M. Hoseini-Athar, R. Mahmudi, R. Prasath Babu, P. Hedström, J. Alloys Compd. 831 (2020) 154766.
[115] M.M. Hoseini-Athar, R. Mahmudi, R. Prasath Babu, P. Hedström, Mater. Sci. Eng. A 808 (2021) 140921.
[116] I. Basu, K.G. Pradeep, C. Mießen, L.A. Barrales-Mora, T. Al-Samman, Acta Mater. 116 (2016) 77–94.
[117] K. Lücke, K. Detert, Acta Metall. 5 (1957) 628–637.
[118] C. Sellars, Q. Zhu, Mater. Sci. Eng. A 280 (2000) 1–7.
[119] M. Kühbach, L. Barrales-Mora, G. Gottstein, Model. Simul. Mater. Sci. Eng. 22 (2014) 075016.
[120] C. Haase, M. Kühbach, L.A. Barrales-Mora, S.L. Wong, F. Roters, D.A. Molodov, G. Gottstein, Acta Mater. 100 (2015) 155–168.
[121] H. Zhang, Y. He, J. Zhang, H. Dong, S. Liu, X. Jiao, R. Wu, X. Zhang, J. Alloy. Compd. 978 (2024) 173473.
[122] J.Y. Zhang, P. Peng, Q.S. Yang, A.A. Luo, J. Magnes. Alloy. 11 (2023) 4407–4419.
[123] S. Wang, H.C. Pan, D.S. Xie, D.D. Zhang, J.R. Li, H.B. Xie, Y.P. Ren, G.W. Qin, J. Magnes. Alloy. 11 (2023) 4128–4145.

[124] M. Kühbach, L. Barrales-Mora, C. Mießen, G. Gottstein, IOP Conf. Ser. Mater. Sci. Eng. 89 (2015) 012031.
[125] R.S. Pei, S. Korte-Kerzel, T. Al-Samman, Mater. Sci. Eng. A 763 (2019) 138112.
[126] R.S. Pei, S. Korte-Kerzel, T. Al-Samman, Materialia 12 (2020) 100715.
[127] R.S. Pei, Y.C. Zou, M. Zubair, D.Q. Wei, T. Al-Samman, Acta Mater. 233 (2022) 117990.
[128] R.S. Pei, S. Korte-Kerzel, T. Al-Samman, J. Mater. Sci. Technol. 50 (2020) 257–270.
[129] S.G. Kim, Y.B. Park, Acta Mater. 56 (2008) 3739–3753.
[130] D.U. Kim, S.G. Kim, W.T. Kim, J.H. Cho, H.N. Han, P.R. Cha, Scr. Mater. 64 (2011) 1079–1082.
[131] S.G. Kim, J.S. Lee, B.J. Lee, Acta Mater. 112 (2016) 150–161.
[132] S.G. Kim, Y.B. Park, Model. Simul. Mater. Sci. Eng. 24 (2016) 065013.
[133] H. Somekawa, D.A. Basha, A. Singh, Materialia 8 (2019) 100466.
[134] H. Somekawa, D. Althaf Basha, A. Singh, T. Tsuru, M. Yamaguchi, Mater. Trans. 61 (2020) 1172–1175.
[135] H. Somekawa, T. Tsuru, A. Singh, Mater. Sci. Eng. A 893 (2024) 146066.
[136] Z. Zhang, J.H. Zhang, W.K. Wang, S.J. Liu, B. Sun, J.S. Xie, T.X. Xiao, Scr. Mater. 221 (2022) 114963.
[137] Z. Zhang, J.S. Xie, J.H. Zhang, H. Dong, S.J. Liu, X.B. Zhang, J. Wang, R.Z. Wu, J. Mater. Sci. Technol. 150 (2023) 49–64.
[138] G.M. Zhu, L.Y. Wang, H. Zhou, J.H. Zhang, Y. Shen, P. Tu, H. Zhu, W. Liu, P.P. Jin, X.Q. Zeng, Int. J. Plast. 120 (2019) 164–179.
[139] I. Basu, M. Chen, J. Wheeler, R.E. Schäublin, J.F. Löffler, Acta Mater. 229 (2022) 117746.
[140] I. Basu, M. Chen, J. Wheeler, R.E. Schäublin, J.F. Löffler, Acta Mater. 211 (2021) 116877.
[141] H.S. Jang, D. Seol, B.J. Lee, J. Alloy. Compd. 894 (2022) 162539.
[142] S.R. Agnew, L. Capolungo, C.A. Calhoun, Acta Mater. 82 (2015) 255–265.
[143] B.Leu K.Yaddanapudi, M.A. Kumar, X. Wang, J.M. Schoenung, E.J. Lavernia, T.J. Rupert, I.J. Beyerlein, S. Mahajan, Acta Mater. 204 (2021) 116514.
[144] Q. Zhu, G. Cao, J.W. Wang, C. Deng, J.X. Li, Z. Zhang, S.X. Mao, Nat. Commun. 10 (2019) 156.
[145] L.H. Wang, Y. Zhang, Z. Zeng, H. Zhou, J. He, P. Liu, M.W. Chen, J. Han, D.J. Srolovitz, J. Teng, Y.Z. Guo, G. Yang, D. Kong, E. Ma, Y.L. Hu, B.C. Yin, X.X. Huang, Z. Zhang, T. Zhu, X.D. Han, Science 375 (2022) 1261–1265.
[146] L. Wang, X. Han, P. Liu, Y. Yue, Z. Zhang, E. Ma, Phys. Rev. Lett. 105 (2010) 135501.
[147] H. Fu, S.Q. Yuan, K.C. Chan, X.S. Yang, Mater. Sci. Eng. A 858 (2022) 144151..
[148] S. Nandy, S.P. Tsai, L. Stephenson, et al., J. Magnes. Alloy. 9 (2021) 1521–1536.
[149] A. Kula, X. Jia, R.K. Mishra, M. Niewczas, Int. J. Plast. 92 (2017) 96–121.
[150] A. Kula, X. Jia, R.K. Mishra, M. Niewczas, Int. J. Plast. 155 (2022) 103321.
[151] A. Kula, K. Noble, R.K. Mishra, M. Niewczas, Philos. Mag. 96 (2016) 134–165.
[152] Y.X. Hua, K.X. Song, H.T. Liu, J.W. Wang, C.M. Zhang, Y.J. Zhou, B. Panga, J.T. Song, J.L. He, H.L. Zhao, J. Mater. Sci. Technol. 159 (2023) 52–61.
[153] R.M. Thomson, Physical Metallurgy in: R.W. Cahn, P. Haasen (Eds.), Elsevier, 1996.
[154] D. McLean, Grain Boundaries in Metals, Clarendon Press, Oxford, UK, 1957.
[155] J.W. Gibbs, Trans. Conn. Acad. Arts Sci. 3 (104–248) (1878) 343–524.
[156] M.A. Gibson, C.A. Schuh, Acta Mater. 95 (2015) 145–155.
[157] X.Y. Qian, Z.H. Dong, B. Jiang, B. Lei, H.B. Yang, C. He, L.T. Liu, C.H. Wang, M. Yuan, H. Yang, B.Q. Yang, C.Y. Zheng, F.S. Pan, Mater. Des. 224 (2022) 111322.
[158] X.Y. Qian, Y.Y. Gao, Z.H. Dong, B. Jiang, C. He, C.H. Wang, A. Zhang, B.Q. Yang, C.Y. Zheng, F.S. Pan, Mater. Sci. Eng. A 867 (2023) 144712.
[159] R.G. Li, S.Q. Zhou, H. Zhang, R.Z. Wu, D. Wu, J.R. Li, B.S. Liu, S.S. Li, X. Li, B.J. Wang, J. Magnes. Alloy. (2023), doi:10.1016/j.jma.2023.03.002.
[160] J.S. Xie, L.L. Wang, J.H. Zhang, L.W. Lu, Z. Zhang, Y.Y. He, R.Z. Wu, J. Magnes. Alloy. 11 (2023) 154–175.
[161] H. Zhang, Y. Li, Z. Ding, T. Xie, R. Liu, Y. Li, D. Zhang, Q. Zhu, X. Shang, X. Zeng, Scr. Mater. 201 (2021) 113982.
[162] J.P. Hirth, J. Lothe, Theory of Dislocations, McGraw-Hill, New York; London, 1968.
[163] H.L. Jia, R. Bjørge, L.F. Cao, H. Song, K. Marthinsen, Y.J. Li, Acta Mater. 155 (2018) 199–213.
[164] E. Nes, B. Holmedal, E. Evangelista, K. Marthinsen, Mater. Sci. Eng. A 410 (2005) 178–182.
[165] S.V. Bobylev, N.A. Enikeev, A.G. Sheinerman, R.Z. Valiev, Int. J. Plast. 123 (2019) 133–144.
[166] N.Q. Vo, J. Schäfer, R.S. Averback, K. Albe, Y. Ashkenazy, P. Bellon, Scr. Mater. 65 (2011) 660–663.
[167] T. Mura, Micromechanics of Defects in Solids, Martinus Nijhoff Publishers, Dordrecht/Boston/Lancaster, 1987.
[168] J.S. Xie, J.H. Zhang, Z. Zhang, Q. Yang, K. Guan, Y.Y. He, R. Wang, H. Zhang, X. Qiu, R.Z. Wu, Corros. Sci. 198 (2022) 110163.
[169] Q.H. Chen, R.N. Chen, J. Su, Q.S. He, B. Tan, C. Xu, X. Huang, Q.W. Dai, J. Lu, J. Magnes. Alloy. 9 (2022) 2384–2397.
[170] B. Kim, C.H. Hong, J.C. Kim, S.Y. Lee, S.M. Baek, H.Y. Jeong, S.S. Park, Scr. Mater. 187 (2020) 24–29.
[171] Z. Li, J. Zhang, T. Xiao, B. Sun, Y. He, S. Liu, L. Liu, Y. Jiao, R. Wu, Mater. Sci. Eng. A 892 (2024) 146059.
[172] Z. Wei, H. Dong, J. Zhang, R. Wu, Y. He, R. Bao, X. Zhang, J. Wang, Mater. Sci. Eng. A 890 (2024) 145842.
[173] Q.Z. Li, J. Magnes. Alloy. 11 (2023) 4420–4430.
[174] X.Z. Li, X.W. Fang, S.P. Wang, S.Q. Wang, M. Zha, K. Huang, J. Magnes. Alloy. 11 (2023) 4644–4658.
[175] J. Zuo, T. Nakata, C. Xu, Y.P. Xia, H.L. Shi, X.J. Wang, G.Z. Tang, W.M. Gan, E. Maawad, G.H. Fan, S. Kamado, L. Geng, Mater. Sci. Eng. A 848 (2022) 143423.
[176] T. Fu, X.Y. Sun, C.C. Ge, D.S. Xie, J.L. Li, H.C. Pan, G.W. Qin, J. Alloy. Compd. 917 (2022) 165407.
[177] H.C. Pan, C. Yang, Y. Yang, Y. Dai, D. Zhou, L. Chai, Q. Huang, Q. Yang, S. Liu, Y. Ren, G. Qin, Mater. Lett. 237 (2019) 65–68.
[178] C. Wang, H. Ning, S. Liu, J. You, T. Wang, H.J. Jia, M. Zha, H.Y. Wang, Scr. Mater. 204 (2021) 114119.
[179] Y.Z. Xu, J.Y. Li, M. Qi, L. Liao, Z. Gao, J. Mater. Res. Technol. 9 (2020) 9856–9867.
[180] L. Zhao, L. Ma, T. Han, G. Qin, H. Duan, Z. Zhao, Mater. Lett. 287 (2021) 129288.
[181] Z. Hua, B. Wang, C. Wang, C. Ma, P. Ma, Z. Guan, Y. Li, J. Li, H. Wang, J. Alloy. Compd. 855 (2021) 157317.
[182] X. Liu, X. Qiao, Z. Li, M. Zheng, Mater. Charact. 162 (2020) 110197.
[183] J. She, S.B. Zhou, P. Peng, A.T. Tang, Y. Wang, H.C. Pan, C.L. Yang, F.S. Pan, Mater. Sci. Eng. A 772 (2020) 138796.
[184] J. Zhao, B. Jiang, Y. Yuan, A. Tang, H. Sheng, T. Yang, G. Huang, D. Zhang, F. Pan, Mater. Sci. Eng. A 772 (2020) 138779.
[185] T. Nakata, T. Mezaki, C. Xu, K. Oh-ishi, K. Shimizu, S. Hanaki, S. Kamado, J. Alloy. Compd. 648 (2015) 428–437.
[186] T. Nakata, C. Xu, Y. Matsumoto, K. Shimizu, T.T. Sasaki, K. Hono, S. Kamado, Mater. Sci. Eng. A 673 (2016) 443–449.
[187] B. Kim, C. Park, H. Kim, B. You, S. Park, Scr. Mater. 76 (2014) 21–24.
[188] T. Nakata, Z.H. Li, T.T. Sasaki, K. Hono, S. Kamado, Scr. Mater. 218 (2022) 114828.
[189] T. Nakata, S. Kamado, J. Magnes. Alloy. 11 (2023) 3992–4010.
[190] T. Nakata, T. Matsuno, R. Oki, S. Kamado, J. Alloy. Compd. 938 (2023) 168519.
[191] T. Nakata, C. Xu, L. Geng, S. Kamado, J. Magnes. Alloy. 11 (2023) 3200–3213.

[192] M.Z. Bian, X.S. Huang, Y. Chino, Acta Mater. 220 (2021) 117328.
[193] D.H. Kang, D.W. Kim, S. Kim, G.T. Ba, K.H. Kim, N.J. Kim, Scr. Mater. 61 (2009) 768–771.
[194] X.L. Wu, M.X. Yang, Yuan F.P, G.L. Wu, Y.J. Wei, X.X. Huang, Y.T. Zhu, Proc. Natl. Acad. Sci. USA 112 (47) (2015) 14501–14505.
[195] Y. Wang, M. Chen, F. Zhou, E. Ma, Nature 419 (2002) 912–915.
[196] Y. Zhu, X. Wu, Mater. Res. Lett. 7 (2019) 393–398.
[197] J. Humphreys, G. Rohrer, A. Rollett, Recrystallization and Related Annealing Phenomena, 3rd ed., Elsevier, 2017.
[198] A. Lakshmanan, M.T. Andani, M. Yaghoobi, J. Allison, A. Misra, V. Sundararaghavan, J. Magnes. Alloy. 11 (2023) 4445–4467.
[199] X.H. Pan, L.F. Wang, P.B. Lu, H. Zhang, G.S. Huang, L.W. Zheng, B. Xing, W.L. Cheng, H.X. Wang, W. Liang, K.S. Shin, J. Magnes. Alloy. 11 (2023) 4659–4678.
[200] Z. Zhang, J.S. Xie, J.H. Zhang, S.J. Liu, R.Z. Wu, X.B. Zhang, J. Mater. Res. Technol. 24 (2023) 5486–5500.